

Angular Distributions of $\bar{B} \rightarrow K\bar{l}l$ Decays

Christoph Bobeth, Gudrun Hiller and Giorgi Piranishvili

Institut für Physik, Technische Universität Dortmund, D-44221 Dortmund, Germany

ABSTRACT: We model-independently analyze the angular distributions of $\bar{B} \rightarrow K\bar{l}l$ decays, $l = e, \mu$, for low dilepton mass using QCD factorization. Besides the decay rate, we study the forward-backward asymmetry A_{FB}^l and a further observable, F_H^l , which gives rise to a flat term in the angular distribution. We find that in the Standard Model $F_H^l \propto m_l^2$, hence vanishing F_H^e and F_H^μ of around 2% (exact value depends on cuts) with a very small theoretical uncertainty of a few percent. We also give predictions for R_K , the ratio of $\bar{B} \rightarrow K\bar{\mu}\mu$ to $\bar{B} \rightarrow K\bar{e}e$ decay rates. We analytically show using large recoil symmetry relations that in the Standard Model R_K equals one up to lepton mass corrections of the order 10^{-4} including α_s and subleading $1/E$ power corrections. The New Physics reach of the observables from the $\bar{B} \rightarrow K\bar{l}l$ angular analysis is explored together with R_K and the $\bar{B}_s \rightarrow \bar{l}l$ and $\bar{B} \rightarrow X_s\bar{l}l$ branching ratios for both $l = e$ and $l = \mu$. We find substantial room for signals from (pseudo-) scalar and tensor interactions beyond the Standard Model. Experimental investigations of the $\bar{B} \rightarrow K\bar{\mu}\mu$ angular distributions are suitable for the LHC environment and high luminosity B factories, where also studies of the electron modes are promising.

KEYWORDS: B-Physics, Beyond Standard Model, Rare Decays.

1. Introduction

The exclusive decays $\bar{B} \rightarrow K\bar{l}l$ with $l = e, \mu$ are governed in the Standard Model (SM) by flavor-changing neutral currents, and hence constitute sensitive probes of New Physics (NP). The three-body decays allow to study non-trivial observables by kinematical measurements of the decay products. They give access to a double differential decay spectrum with respect to the invariant mass of the lepton pair q^2 and a lepton charge asymmetry angle $\cos\theta$. In the absence of large statistics, partially integrated spectra such as the dilepton mass spectrum $d\Gamma_l/dq^2$ or the angular distribution $d\Gamma_l/d\cos\theta$ can be explored. Further $\Gamma_l \equiv \Gamma(\bar{B} \rightarrow K\bar{l}l)$ is in general different for electrons and muons. Having various theoretical or experimental advantages, the $\bar{B} \rightarrow K\bar{l}l$ observables cover a wide range of SM tests and NP searches, that are well suited for experimental study at high luminosity facilities at the $\Upsilon(4S)$ and the Large Hadron Collider (LHC), e.g., [1].

The $\bar{B} \rightarrow K\bar{l}l$ branching ratio has been determined experimentally to be in agreement with the SM within uncertainties, and lies in the 10^{-7} region [2, 3, 4, 5, 6]. Early data on more elaborate observables and q^2 -spectra are beginning to come from the B factories [2, 3, 4]. While theoretical studies presented extensive phenomenological analyses of the dilepton mass distribution [6, 7], a detailed exploration of the SM background and NP potential of the angular dependence in the decay distribution is lacking. The $\bar{B} \rightarrow K\bar{l}l$ angular distribution is very simple in the SM [6, 7]

$$\frac{d\Gamma_l^{\text{SM}}}{d\cos\theta} \propto \sin^2\theta + \mathcal{O}(m_l^2), \quad (1.1)$$

up to small lepton mass corrections of kinematical origin. A closer analysis shows that the $\cos\theta$ -dependence of the (normalized) angular distribution can be parametrized as [4, 6, 7]

$$\frac{1}{\Gamma_l} \frac{d\Gamma_l}{d\cos\theta} = \frac{3}{4}(1 - F_H^l)(1 - \cos^2\theta) + \frac{1}{2}F_H^l + A_{\text{FB}}^l \cos\theta, \quad (1.2)$$

with a flat term $F_H^l/2$ and a linear term in $\cos\theta$, the forward-backward asymmetry A_{FB}^l . Both are small within the SM, and therefore can signal the presence of NP. In particular they can be affected by Higgs and tensor interactions. Note that in the limit of vanishing lepton masses the SM predicts the same rates for electrons and muons $\Gamma_e^{\text{SM}} = \Gamma_\mu^{\text{SM}} + \mathcal{O}(m_\mu^2)$ if the same kinematical cuts are used [8].

In this paper we analyze the angular distributions of $\bar{B} \rightarrow K\bar{l}l$ decays. We explicitly quantify the corrections to (1.1) within the SM and study model-independently the effects of $(\bar{s}b)(\bar{l}l)$ operators induced by physics beyond the SM on (1.2). We use the framework of QCD factorization (QCDF) valid in the low- q^2 region [9, 10] and exploit the symmetries of QCD in the large recoil limit of heavy-to-light transitions [11, 12]. Also, resonance contributions from $\bar{B} \rightarrow K(c\bar{c}) \rightarrow K\bar{l}l$ can be controlled for dilepton masses below the charm threshold.

The plan of the paper is as follows: After setting up the effective weak Hamiltonian in Section 2 hadronic matrix elements are given in Section 3. Section 4 contains model-independent formulae of the double differential and angular decay distributions. We give

numerical predictions for the SM in Section 5 including a detailed discussion of uncertainties. We also derive analytical expressions for Γ_l and F_H^l obtained in the large recoil limit. In Section 6 we work out the sensitivity of the $\bar{B} \rightarrow K\bar{l}l$ angular distributions to NP in correlation with other observables in $b \rightarrow s\bar{l}l$ decays. We summarize in Section 7. Technical details about form factors and form factor symmetry relations in the low- q^2 region are given in Appendix A, whereas details on the $\bar{B} \rightarrow K\bar{l}l$ hadronic matrix element in QCDF can be found in Appendix B.

2. The Effective Hamiltonian

The $\Delta B = 1$ effective Hamiltonian

$$\mathcal{H}_{\text{eff}} = -\frac{4G_F}{\sqrt{2}}V_{tb}V_{ts}^* \sum_i C_i(\mu)\mathcal{O}_i(\mu) \quad (2.1)$$

is given in terms of dimension six operators \mathcal{O}_i and their respective Wilson coefficients C_i . Both depend on the renormalization scale μ , for which we take a low energy scale μ_b of the order of the b -quark mass when evaluating B -physics amplitudes. In (2.1) the leading CKM elements V_{lm} are factored out. The sum over i comprises the current-current operators $i = 1, 2$, the QCD-penguin operators $i = 3, 4, 5, 6$, the photon and gluon dipole operators $i = 7, 8$ and the semileptonic operators $i = 9, 10$. They are defined as

$$\begin{aligned} \mathcal{O}_7 &= \frac{e}{(4\pi)^2}\bar{m}_b[\bar{s}\sigma^{\mu\nu}P_R b]F_{\mu\nu}, & \mathcal{O}_9 &= \frac{e^2}{(4\pi)^2}[\bar{s}\gamma_\mu P_L b][\bar{l}\gamma^\mu l], \\ \mathcal{O}_8 &= \frac{g_s}{(4\pi)^2}\bar{m}_b[\bar{s}\sigma^{\mu\nu}P_R T^a b]G_{\mu\nu}^a, & \mathcal{O}_{10} &= \frac{e^2}{(4\pi)^2}[\bar{s}\gamma_\mu P_L b][\bar{l}\gamma^\mu\gamma_5 l], \end{aligned} \quad (2.2)$$

where $P_{R/L} = (1 \pm \gamma_5)/2$ denote chiral projectors and $\bar{m}_b(\mu)$ the $\overline{\text{MS}}$ b -quark mass at the scale μ . For the operators \mathcal{O}_i with $i = 1, \dots, 6$ we use the definitions given in [13], also used by [9, 10]. This set of operators suffices to describe $b \rightarrow s\bar{l}l$ induced processes in the SM, which are dominated by C_7, C_9 and C_{10} , whereas C_8 enters at higher order in the strong coupling.

Beyond the SM, NP might contribute in various ways. Assuming that NP manifests itself at and above the electroweak scale, it can be model-independently analyzed in the effective theory framework by allowing for NP contributions to the Wilson coefficients of the SM operators and by additional operators not present in the SM. To account also for the latter we include the most general $b \rightarrow s$ (pseudo-) scalar and tensor operators with dileptons into our analysis:

$$\begin{aligned} \mathcal{O}_S^l &= \frac{e^2}{(4\pi)^2}[\bar{s}P_R b][\bar{l}l], & \mathcal{O}_S^{\prime l} &= \frac{e^2}{(4\pi)^2}[\bar{s}P_L b][\bar{l}l], \\ \mathcal{O}_P^l &= \frac{e^2}{(4\pi)^2}[\bar{s}P_R b][\bar{l}\gamma_5 l], & \mathcal{O}_P^{\prime l} &= \frac{e^2}{(4\pi)^2}[\bar{s}P_L b][\bar{l}\gamma_5 l], \\ \mathcal{O}_T^l &= \frac{e^2}{(4\pi)^2}[\bar{s}\sigma_{\mu\nu} b][\bar{l}\sigma^{\mu\nu} l], & \mathcal{O}_{T5}^l &= \frac{e^2}{(4\pi)^2}[\bar{s}\sigma_{\mu\nu} b][\bar{l}\sigma^{\mu\nu}\gamma_5 l], \end{aligned} \quad (2.3)$$

where we made the dependence on the lepton flavor explicit by the superscript l . Note that there are only two independent tensor operators in four dimensions. At higher order also 4-quark operators with scalar, pseudoscalar and tensorial structure contribute to rare radiative and semileptonic decays [8, 14]. Here we neglect these effects.

The additional NP operators (2.3) mix under QCD only with themselves. Their 1-loop anomalous dimensions $\gamma_i = \frac{\alpha_s}{4\pi}\gamma_i^{(0)}$ are

$$\begin{aligned}\gamma_i^{(0)} &= -6C_F = -8, & i &= S, S', P, P', \\ \gamma_i^{(0)} &= 2C_F = \frac{8}{3}, & i &= T, T5.\end{aligned}\tag{2.4}$$

In our NP analyses all Wilson coefficients are taken at the low scale μ_b .

3. The Hadronic Matrix Element at Large Recoil

A systematic treatment of the matrix element $\mathcal{M}[\bar{B} \rightarrow K\bar{l}l] = \langle l(p_-)\bar{l}(p_+)K(p_K)|\mathcal{H}_{\text{eff}}|\bar{B}(p_B)\rangle$ is available in the large recoil region. We denote by p_B, p_K, p_- and p_+ the 4-momenta of the \bar{B} -meson, kaon, lepton l and antilepton \bar{l} , respectively, and M_B, M_K and m_l are the corresponding masses. At large recoil the energy E of the K -meson is large compared to the typical size of hadronic binding energies $\Lambda_{\text{QCD}} \ll E$ and the dilepton invariant mass squared $q^2 = (p_- + p_+)^2$ is low, $q^2 \ll M_B^2$. Consequently, in this region the virtual photon exchange between the hadronic part and the dilepton pair and hard gluon scattering can be treated in an expansion in $1/E$ using either QCDF or Soft Collinear Effective Theory (SCET) [15]. Furthermore, only one soft form factor $\xi_P(q^2)$ appears in the $\bar{B} \rightarrow K$ heavy-to-light decay amplitude due to symmetry relations in the large energy limit of QCD [11, 12]. Other nonperturbative objects present are the light-cone distribution amplitudes (LCDAs) of the \bar{B} - and K -mesons, leading to numerically smaller contributions. This framework has been previously applied to $\bar{B} \rightarrow K^*\bar{l}l$ decays using QCDF [9, 10] or SCET [16]. In this work we use the results from QCDF valid at low q^2 [9, 10] and include effects of finite lepton masses in $\bar{B} \rightarrow K\bar{l}l$ decays.

The $\bar{B} \rightarrow K\bar{l}l$ matrix element can be written as

$$\begin{aligned}\mathcal{M}[\bar{B} \rightarrow K\bar{l}l] &= i\frac{G_F\alpha_e}{\sqrt{2}\pi}V_{tb}V_{ts}^*\xi_P(q^2)\left(F_V p_B^\mu[\bar{l}\gamma_\mu l] + F_A p_B^\mu[\bar{l}\gamma_\mu\gamma_5 l] \right. \\ &\quad \left. + (F_S + \cos\theta F_T)[\bar{l}l] + (F_P + \cos\theta F_{T5})[\bar{l}\gamma_5 l]\right).\end{aligned}\tag{3.1}$$

Here, θ denotes the angle between the direction of motion of the \bar{B} and the negatively charged lepton l in the dilepton center of mass frame, following [7]. Note that this convention differs from other works, e.g., [6], where θ is defined with respect to \bar{l} . The functions $F_i \equiv F_i(q^2)$, $i = S, P, A, V, T, T5$ are given as

$$F_A = C_{10}, \quad F_T = \frac{2\sqrt{\lambda}\beta_l}{M_B + M_K}\frac{f_T(q^2)}{f_+(q^2)}C_T^l, \quad F_{T5} = \frac{2\sqrt{\lambda}\beta_l}{M_B + M_K}\frac{f_T(q^2)}{f_+(q^2)}C_{T5}^l,$$

$$F_P = \frac{1}{2} \frac{M_B^2 - M_K^2}{m_b - m_s} \frac{f_0(q^2)}{f_+(q^2)} (C_P^l + C_P^{\prime l}) + m_l C_{10} \left[\frac{M_B^2 - M_K^2}{q^2} \left(\frac{f_0(q^2)}{f_+(q^2)} - 1 \right) - 1 \right], \quad (3.2)$$

$$F_S = \frac{1}{2} \frac{M_B^2 - M_K^2}{m_b - m_s} \frac{f_0(q^2)}{f_+(q^2)} (C_S^l + C_S^{\prime l}), \quad F_V = C_9 + \frac{2m_b}{M_B} \frac{\mathcal{T}_P(q^2)}{\xi_P(q^2)} + \frac{8m_l}{M_B + M_K} \frac{f_T(q^2)}{f_+(q^2)} C_T^l,$$

where

$$\lambda = M_B^4 + M_K^4 + q^4 - 2(M_B^2 M_K^2 + M_B^2 q^2 + M_K^2 q^2), \quad \beta_l = \sqrt{1 - 4 \frac{m_l^2}{q^2}}, \quad (3.3)$$

and it is useful to note that $2p_B \cdot (p_+ - p_-) = \sqrt{\lambda} \beta_l \cos \theta$. In the SM holds $F_S^{\text{SM}} = F_T^{\text{SM}} = F_{T_5}^{\text{SM}} = 0$. Above, we have written the matrix element with the form factor $\xi_P(q^2) = f_+(q^2)$ as an overall factor. It constitutes the main source of theoretical uncertainties. The form factor ratios f_0/f_+ and f_T/f_+ are constrained by symmetry relations at large recoil [11, 12], which are given in Appendix A together with definitions of the form factors and a discussion of their uncertainties. The quantity $\mathcal{T}_P(q^2)$ appearing in the vector coupling to leptons, F_V , takes into account virtual one-photon exchange between the hadrons and the lepton pair and hard scattering contributions. $\mathcal{T}_P(q^2)$ can be extracted from [9] and is given in Appendix B. At lowest order (denoted by the superscript (0)) up to numerically small annihilation contributions, it reads as

$$\mathcal{T}_P^{(0)}(q^2) = \xi_P(q^2) \left[C_7^{\text{eff}(0)} + \frac{M_B}{2m_b} Y^{(0)}(q^2) \right]. \quad (3.4)$$

Hence, $\mathcal{T}_P(q^2)$ takes care of the contributions from the $\mathcal{O}_{1,\dots,6}$ matrix elements $\propto Y(q^2)$ that are commonly included in an effective coefficient of the operator \mathcal{O}_9 [17]. The next-to leading α_s -corrections to \mathcal{T}_P are known, see Appendix B, and taken into account in our analysis. Here we consider only NP effects from the NP operators (2.3), that is, their respective coefficients as appearing in (3.2) being non-zero, and \mathcal{T}_P is SM-like. The b -quark mass in \mathcal{T}_P and F_V is the potential subtracted (PS) mass $m_b^{\text{PS}}(\mu_f)$ at the factorization scale $\mu_f \sim \sqrt{\Lambda_{\text{QCD}} m_b}$ and is denoted by m_b throughout the paper. The b -quark mass factors in F_S and F_P stem from the equations of motion, and we take them in the PS scheme as well. In the evaluation of the function $Y(q^2)$ we use the pole mass m_b^{pole} [9]. The relation to the PS mass is given as $m_b^{\text{pole}} = m_b^{\text{PS}}(\mu_f) + 4\alpha_s \mu_f / (3\pi)$ [18]. The SM Wilson coefficients C_9 and C_{10} are taken in NNLL approximation [13, 19]. The remaining SM Wilson coefficients $C_{1,\dots,6}$ and $C_{7,8}$ with their effective counterparts $C_{7,8}^{\text{eff}}$ enter only through \mathcal{T}_P . For details see Appendix B and [9]. Note that chirality flipped operators $\mathcal{O}_{7,9,10}^{\prime}$ can be readily included in the matrix element of $\bar{B} \rightarrow K \bar{l} l$ decays by replacing $C_{9,10} \rightarrow C_{9,10} + C_{9,10}^{\prime}$ in (3.2) and $C_7 \rightarrow C_7 + C_7^{\prime}$ in \mathcal{T}_P .

4. Decay Distributions of $\bar{B} \rightarrow K\bar{l}l$

Based on the matrix element (3.1) the double differential decay rate with respect to q^2 and $\cos \theta$ with lepton flavor l reads as

$$\frac{d^2\Gamma_l}{dq^2 d\cos \theta} = a_l(q^2) + b_l(q^2) \cos \theta + c_l(q^2) \cos^2 \theta, \quad (4.1)$$

where

$$\begin{aligned} \frac{a_l(q^2)}{\Gamma_0 \sqrt{\lambda} \beta_l \xi_P^2} &= q^2 (\beta_l^2 |F_S|^2 + |F_P|^2) + \frac{\lambda}{4} (|F_A|^2 + |F_V|^2) \\ &\quad + 2m_l (M_B^2 - M_K^2 + q^2) \text{Re}(F_P F_A^*) + 4m_l^2 M_B^2 |F_A|^2, \end{aligned} \quad (4.2)$$

$$\begin{aligned} \frac{b_l(q^2)}{\Gamma_0 \sqrt{\lambda} \beta_l \xi_P^2} &= 2 \left\{ q^2 [\beta_l^2 \text{Re}(F_S F_T^*) + \text{Re}(F_P F_{T5}^*)] \right. \\ &\quad \left. + m_l [\sqrt{\lambda} \beta_l \text{Re}(F_S F_V^*) + (M_B^2 - M_K^2 + q^2) \text{Re}(F_{T5} F_A^*)] \right\}, \end{aligned} \quad (4.3)$$

$$\frac{c_l(q^2)}{\Gamma_0 \sqrt{\lambda} \beta_l \xi_P^2} = q^2 (\beta_l^2 |F_T|^2 + |F_{T5}|^2) - \frac{\lambda}{4} \beta_l^2 (|F_A|^2 + |F_V|^2) + 2m_l \sqrt{\lambda} \beta_l \text{Re}(F_T F_V^*) \quad (4.4)$$

and

$$\Gamma_0 = \frac{G_F^2 \alpha_e^2 |V_{tb} V_{ts}^*|^2}{512 \pi^5 M_B^3}. \quad (4.5)$$

These relations simplify considerably in the SM, where $b_l^{\text{SM}}(q^2) = 0$ and in the limit $m_l \rightarrow 0$ further holds $a_l^{\text{SM}}(q^2) = -c_l^{\text{SM}}(q^2)$.

With (4.1) at hand the angular distribution

$$\frac{d\Gamma_l}{d\cos \theta} = A_l + B_l \cos \theta + C_l \cos^2 \theta \quad (4.6)$$

is given in terms of the q^2 -integrated coefficients

$$A_l = \int_{q_{\min}^2}^{q_{\max}^2} dq^2 a_l(q^2), \quad B_l = \int_{q_{\min}^2}^{q_{\max}^2} dq^2 b_l(q^2), \quad C_l = \int_{q_{\min}^2}^{q_{\max}^2} dq^2 c_l(q^2). \quad (4.7)$$

Their values depend on the cuts in q^2 . We recall that while the boundaries of the phase space allow for dilepton masses in the range $4m_l^2 < q^2 \leq (M_B - M_K)^2$, our calculation is valid only in the low- q^2 region. Note that for very low dilepton masses there is sensitivity to light resonances. We therefore restrict our analysis to $1 \text{ GeV}^2 \lesssim q^2 < 7 \text{ GeV}^2$.

The decay rate Γ_l and the integrated and normalized forward-backward asymmetry A_{FB}^l of the lepton pair can be expressed in terms of A_l, B_l and C_l

$$\Gamma_l = 2 \left(A_l + \frac{1}{3} C_l \right), \quad A_{\text{FB}}^l = \frac{B_l}{\Gamma_l}. \quad (4.8)$$

We further introduce the observable

$$F_H^l \equiv \frac{2}{\Gamma_l} (A_l + C_l) = \int_{q_{\min}^2}^{q_{\max}^2} dq^2 [a_l(q^2) + c_l(q^2)] \Big/ \int_{q_{\min}^2}^{q_{\max}^2} dq^2 \left[a_l(q^2) + \frac{1}{3} c_l(q^2) \right]. \quad (4.9)$$

With (4.8) and (4.9), the angular distribution (4.6) is equivalent to (1.2) presented in the Introduction. Since F_H^l is normalized to Γ_l , we expect reduced uncertainties in the former compared to the latter due to cancellations between numerator and denominator. As already anticipated after (4.5) within the SM a cancellation takes place in (4.9) between a_l and c_l such that $F_H^{l\text{SM}}$ vanishes in the limit $m_l \rightarrow 0$. We discuss this in detail in the next section. From here follows the approximate $\propto \sin^2 \theta$ angular dependence of $\bar{B} \rightarrow K\bar{l}l$ decays in the SM as in (1.1).

We would like to comment on the possibility of corrections to (1.2) or (4.6) from higher powers of $\cos \theta$, that is, a polynomial dependence in the angular distribution on $\cos^n \theta$ with $n > 2$. Higher angular momenta arise from higher (> 6) dimensional operators in the weak Hamiltonian (2.1) or from QED corrections. Hence, they are suppressed by powers of external low energy momenta or masses over the electroweak scale, and $\alpha_e/4\pi$, respectively. We discuss such corrections further at the end of Section 5 in the context of a non-vanishing forward-backward asymmetry in $\bar{B} \rightarrow K\bar{l}l$ in the SM.

A further useful observable in $\bar{B} \rightarrow K\bar{l}l$ decays is R_K , the ratio of $\bar{B} \rightarrow K\bar{\mu}\mu$ to $\bar{B} \rightarrow K\bar{e}e$ decay rates with the same q^2 cuts [8]

$$R_K \equiv \frac{\Gamma_\mu}{\Gamma_e} = \int_{q_{\min}^2}^{q_{\max}^2} dq^2 \frac{d\Gamma_\mu}{dq^2} \Big/ \int_{q_{\min}^2}^{q_{\max}^2} dq^2 \frac{d\Gamma_e}{dq^2} = \frac{\Gamma_\mu F_H^\mu - 4/3 C_\mu}{\Gamma_e}, \quad (4.10)$$

which probes lepton flavor dependent effects in and beyond the SM. We find that F_H^l and R_K are model-independently related

$$R_K \cdot (1 - F_H^\mu - \Delta) = 1, \quad \text{where} \quad \Delta = \frac{4 C_e - C_\mu}{3 \Gamma_\mu} - \frac{F_H^e}{R_K}. \quad (4.11)$$

The expression for Δ simplifies in models where chiral couplings to electrons can be neglected as, for example, in the SM with $m_e = 0$. Then $F_H^e = 0$ and $\Gamma_e = -4/3 C_e$ and in the SM $\Delta^{\text{SM}} \propto m_\mu^2$. We carefully examine SM predictions for Γ_l , F_H^l and R_K in Section 5 and work out the NP potential of R_K , F_H^l and A_{FB}^l in Section 6. Corresponding values for Δ can be obtained by means of (4.11).

5. Standard Model Predictions

In this section we analyze $\bar{B} \rightarrow K\bar{l}l$ decays within the SM. We give predictions for the observables F_H^l , R_K and Γ_l and the corresponding branching ratios $\mathcal{B}_l \equiv \mathcal{B}(\bar{B} \rightarrow K\bar{l}l)$ for low dilepton mass. Higher order SM contributions to the forward-backward asymmetry A_{FB}^l are briefly discussed.

We start with a general analysis of lepton flavor dependence in the $\bar{B} \rightarrow K\bar{l}l$ decay rate Γ_l . In the SM, such effects are of purely kinematical origin and often negligible [8]. At

large recoil, the suppression of the lepton mass induced terms can be quantified analytically using form factor symmetry relations (A.3). For low q^2 , Γ_l can then be written as

$$\Gamma_l^{\text{SM}} = \frac{\Gamma_0}{3} \int_{q_{\text{min}}^2}^{q_{\text{max}}^2} dq^2 \xi_P^2(q^2) \sqrt{\lambda}^3 (|F_A|^2 + |F_V|^2) \quad (5.1)$$

$$\times \left\{ 1 + \mathcal{O}\left(\frac{m_l^4}{q^4}\right) + \frac{m_l^2}{M_B^2} \times \mathcal{O}\left(\alpha_s, \frac{q^2}{M_B^2} \sqrt{\frac{\Lambda_{\text{QCD}}}{E}}\right) \right\},$$

where the m_l^4 correction has been obtained from explicit expansion of the coefficients a_l (4.2) and c_l (4.4) in m_l . (A useful relation is given in (A.4).) Due to a cancellation with the kinematical function β_l there are no terms of order m_l^2 up to symmetry breaking corrections, which are estimated in the second correction term in (5.1). Form factor relations are broken in general by α_s -corrections and power corrections in Λ_{QCD}/E , as discussed in more detail in Appendix A. As can be seen, these receive here further strong suppression from m_l^2/M_B^2 . Note that consistent with the Λ_{QCD}/E expansion we neglected terms of order M_K^2/M_B^2 and we approximated in the symmetry breaking correction contribution in (5.1) $\lambda \approx M_B^4$, thereby dropping terms suppressed by q^2/M_B^2 .

We conclude from (5.1) that lepton mass effects in the SM $\bar{B} \rightarrow K\bar{l}$ decay rate at low q^2 are of order $m_\mu^4/q^4 \sim 10^{-4}$ for muons and even further down by $m_e^2/m_\mu^2 \simeq 2 \cdot 10^{-5}$ for electrons, hence negligible in agreement with earlier numerical findings covering the whole dilepton mass region [8]. To leading order in m_l , the decay rate depends then only on $|F_V|$ and $|F_A|$. The function F_A equals the Wilson coefficient $C_{10}^{\text{SM}} \sim -4$ with tiny dependence on the low scale μ_b . F_V is a sum of $C_9^{\text{SM}} \sim +4$ and a term containing \mathcal{T}_P . The latter is subject to unknown higher order power corrections. However, the typical order of magnitude of $|\mathcal{T}_P(q^2)| \sim 0.1$ implies that these corrections constitute a rather small contribution to F_V and the corresponding uncertainties are very small compared to the dominating one from the overall form factor ξ_P .

The numerical analysis of Γ_l confirms the discussed qualitative features. The main uncertainties are due to the form factor ξ_P , the CKM matrix element V_{ts} and the renormalization scale μ_b . For the form factor $\xi_P(q^2)$ we use the findings from Light Cone Sum Rules (LCSR) [26]. At low dilepton mass, the form factor has an uncertainty between (12 – 16)%, with smaller uncertainty for larger q^2 , for details see Appendix A. Our numerical input is given in Table 1. We find that the μ_b -dependence of the decay rate is rather small, about a few percent, as can be seen from Figure 1 (left-hand plot). Here the coefficients $a_\mu(q^2)$ and, to enable easier comparison, $-c_\mu(q^2)$ are shown for μ_b between $m_b/2$ and $2m_b$. The small uncertainty due to μ_b is not unexpected because of the inclusion of NNLL corrections to the matrix elements of the current-current operators [27] in \mathcal{T}_P , which cancels the μ_b -dependence of C_9^{SM} . In the right-hand plot of Figure 1 we show Γ_μ for three lower cuts $q_{\text{min}}^2 = \{0.5, 1, 2\}$ GeV² as a function of the upper boundary q_{max}^2 . The combined uncertainty from $\xi_P(q^2)$, μ_b and V_{ts} can be as large as 32%. Further subleading sources are the lifetime with 0.7% uncertainty and $\alpha_e(\mu)$, which enters quadratically and brings in about 6% uncertainty to the $\bar{B} \rightarrow K\bar{l}$ decay rates. The latter can be reduced by including the higher order electroweak corrections from [28, 29] to the renormalization

$\alpha_s(m_Z) = 0.1176 \pm 0.0020$	[20]	$f_K = (159.8 \pm 1.4 \pm 0.44) \text{ MeV}$	[20]
$\alpha_e(m_b) = 1/133$		$f_{B_{u,d}} = (200 \pm 30) \text{ MeV}$	
$ V_{ts} = 0.0409 \pm 0.0021$	[21]	$f_{B_s} = (240 \pm 30) \text{ MeV}$	[23]
$ V_{cb} = 0.0416 \pm 0.0007$	[21]	$a_1^K(1 \text{ GeV}) = 0.06 \pm 0.03$	[25]
$m_W = 80.403 \text{ GeV}$	[20]	$a_2^K(1 \text{ GeV}) = 0.25 \pm 0.15$	[25]
$m_t^{pole} = (170.9 \pm 1.8) \text{ GeV}$	[22]	$a_4^K(1 \text{ GeV}) = -0.015 \pm 0.1$	[26]
$m_b = (4.6 \pm 0.1) \text{ GeV}$	[9]	$\lambda_{B,+}(1.5 \text{ GeV}) = (0.458 \pm 0.115) \text{ GeV}$	[10, 24]
$m_c^{pole} = (1.4 \pm 0.2) \text{ GeV}$		$\xi_P(0) = 0.327 \pm 0.053$	[25, 26]
$\mathcal{B}(\bar{B} \rightarrow X_c l \bar{\nu}_l) = (10.57 \pm 0.15)\%$	[20]	$\tau_{B^\pm} = (1.638 \pm 0.011) \text{ ps}$	[20]
		$\tau_{B^0} = (1.530 \pm 0.009) \text{ ps}$	[20]
		$\tau_{B_s} = (1.425 \pm 0.041) \text{ ps}$	[20]

Table 1: The numerical input used in our analysis. We denote by m_b the PS mass at the factorization scale $\mu_f = 2 \text{ GeV}$. We neglect the strange quark mass throughout this work.

group evolution which should capture the leading effect. For a complete higher order electroweak analysis the QED-corrections to the $\bar{B} \rightarrow K \bar{l} l$ matrix element should be calculated. In the corresponding calculation for inclusive $\bar{B} \rightarrow X_s \bar{l} l$ decays collinear logarithms of order $\alpha_e/(4\pi) \cdot \log(m_l/m_b)$ arise for low dilepton mass cuts [29]. The resulting splitting between electron and muon final states, however, diminishes after experimental cuts which separate electrons from energetic collinear photons. How much this matters for Γ_e and Γ_μ and R_K cannot be answered until these QED-corrections are calculated. The uncertainties in Γ_l from the charm, bottom and top mass are 2%, 0.4% and 2%, respectively.

In Table 2 predictions for the SM branching ratios of $B^- \rightarrow K^- \bar{\mu} \mu$ and $\bar{B}^0 \rightarrow K^0 \bar{\mu} \mu$ decays are given including the uncertainties from $\xi_P(q^2)$, V_{ts} and μ_b added in quadrature. The relative errors due to ξ_P and μ_b are given also separately. Lepton mass effects are negligible in Γ_l and \mathcal{B}_l , and the decay rates and branching ratios with electrons agree within uncertainties with the corresponding ones with muons. The splitting of (9.5–9.7)% between the branching ratios of the B^- and \bar{B}^0 mesons is dominated by the lifetime difference, but there is also a small isospin breaking contribution from spectator effects residing in \mathcal{T}_P .

In view of the insensitivity of Γ_l^{SM} to lepton mass effects for $l = e, \mu$ and with regard to its large form factor uncertainty it was proposed in [8] to investigate the ratio Γ_μ/Γ_e , i.e., R_K (4.10). Our numerical analysis confirms a cancellation of the hadronic uncertainties in R_K also for low dilepton mass as can be seen in Figure 2. Here we show R_K for different cuts $q_{\text{min}}^2 = \{0.5, 1, 2\} \text{ GeV}^2$ versus q_{max}^2 . The combined uncertainty due to the form factor $\xi_P(q^2)$ and the renormalization scale μ_b is given by the bands and is tiny. This can be seen also from Table 2. The μ_b and $\xi_P(q^2)$ induced uncertainties in R_K are of comparable size, of the order $\lesssim 10^{-4}$. The deviation of R_K^{SM} from 1 is mainly due to the inclusion of effects of $\mathcal{O}(m_\mu^4/q^4) \sim 10^{-4}$ given in (5.1). Any measured deviation of R_K from 1 thus will signal NP which does not contribute equally to Γ_μ and Γ_e as, for example, in the presence of non-universal lepton couplings.

Similar to R_K also the angular observable F_H^l (4.9) is a ratio, where the overall factor

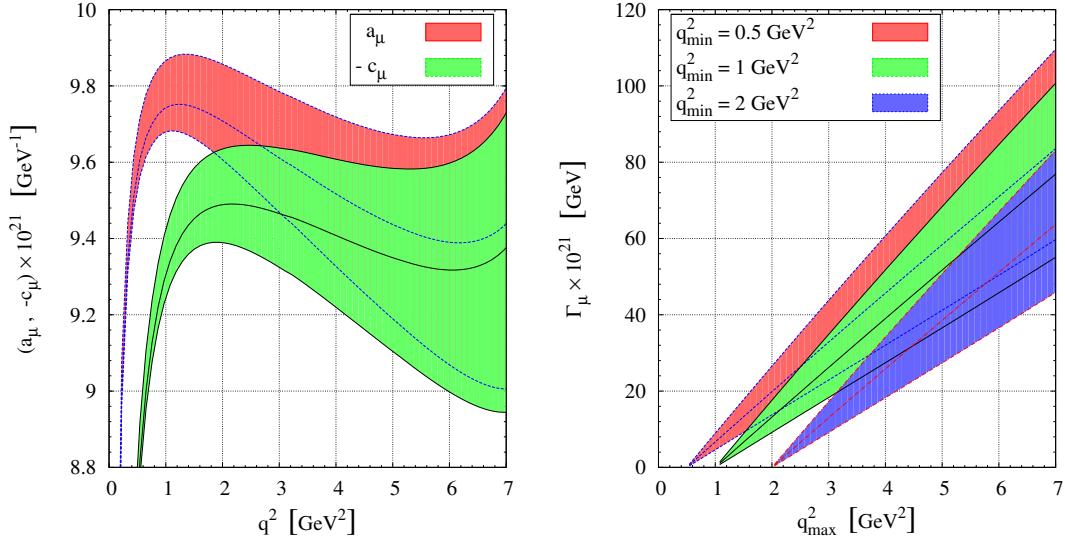


Figure 1: In the left-hand plot $a_l(q^2)$ and $-c_l(q^2)$ defined in (4.1) are shown for $l = \mu$ in the SM as a function of q^2 for the renormalization scale μ_b between $m_b/2$ and $2m_b$. In the right-hand plot the SM $\bar{B} \rightarrow K\bar{\mu}\mu$ decay rate is given for three different cuts $q_{\text{min}}^2 = \{0.5, 1, 2\} \text{ GeV}^2$ as a function of q_{max}^2 . Here the bands take into account uncertainties from the form factor ξ_P , μ_b and V_{ts} .

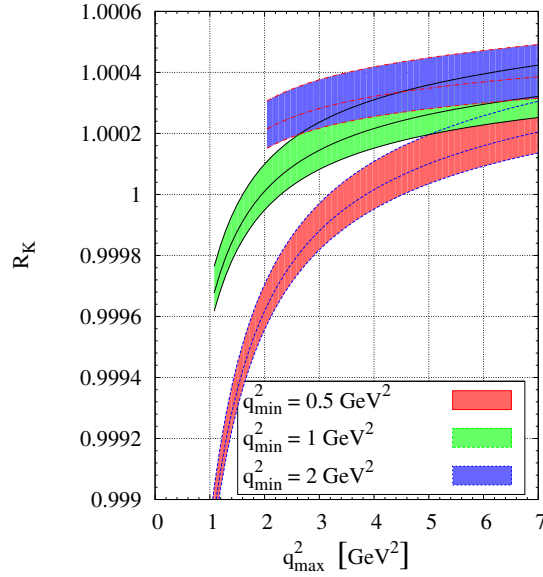


Figure 2: The ratio R_K in the SM for different cuts $q_{\text{min}}^2 = \{0.5, 1, 2\} \text{ GeV}^2$ as a function of q_{max}^2 . The uncertainties from the scale μ_b and the form factor are added in quadrature.

Γ_0 (4.5) drops out and uncertainties can cancel. With the aid of the form factor symmetry

	$B^- \rightarrow K^- \bar{l}$			$\bar{B}^0 \rightarrow K^0 \bar{l}$		
	SM value	ξ_P [%]	μ_b [%]	SM value	ξ_P [%]	μ_b [%]
\mathcal{B}_μ [10^{-7}]	$1.60^{+0.51}_{-0.46}$	+29.9 -27.0	+2.0 -1.8	$1.46^{+0.47}_{-0.43}$	+30.4 -27.4	+2.1 -2.0
	$1.27^{+0.40}_{-0.36}$	+29.4 -26.6	+2.2 -2.1	$1.16^{+0.37}_{-0.33}$	+29.8 -27.0	+2.3 -2.2
	$1.91^{+0.59}_{-0.54}$	+29.2 -26.6	+2.2 -2.2	$1.74^{+0.55}_{-0.50}$	+29.6 -26.8	+2.3 -2.3
	$1.59^{+0.48}_{-0.44}$	+28.7 -26.0	+2.4 -2.4	$1.45^{+0.45}_{-0.41}$	+29.0 -26.3	+2.5 -2.6
F_H^μ	$0.0244^{+0.0003}_{-0.0003}$	+0.8 -1.0	+0.7 -0.5	$0.0243^{+0.0003}_{-0.0003}$	+0.9 -1.1	+0.7 -0.4
	$0.0188^{+0.0002}_{-0.0001}$	+0.4 -0.5	+0.7 -0.4	$0.0187^{+0.0002}_{-0.0001}$	+0.5 -0.5	+0.7 -0.4
	$0.0221^{+0.0003}_{-0.0003}$	+1.2 -1.4	+0.9 -0.6	$0.0221^{+0.0003}_{-0.0004}$	+1.2 -1.5	+0.9 -0.6
	$0.0172^{+0.0002}_{-0.0002}$	+0.7 -0.8	+0.9 -0.6	$0.0172^{+0.0002}_{-0.0002}$	+0.7 -0.8	+0.9 -0.6
R_K	$1.00030^{+0.00010}_{-0.00007}$	+0.004 -0.003	+0.010 -0.006	$1.00031^{+0.00010}_{-0.00007}$	+0.004 -0.003	+0.010 -0.006
	$1.00037^{+0.00010}_{-0.00007}$	+0.004 -0.003	+0.010 -0.006	$1.00038^{+0.00011}_{-0.00007}$	+0.004 -0.003	+0.010 -0.006
	$1.00032^{+0.00010}_{-0.00007}$	+0.004 -0.003	+0.010 -0.006	$1.00033^{+0.00011}_{-0.00007}$	+0.004 -0.003	+0.010 -0.006
	$1.00039^{+0.00011}_{-0.00007}$	+0.004 -0.003	+0.010 -0.006	$1.00040^{+0.00011}_{-0.00007}$	+0.004 -0.003	+0.010 -0.007

Table 2: SM predictions for \mathcal{B}_μ (in units of 10^{-7}), F_H^μ and R_K for charged and neutral B -meson decays and different q^2 cuts $(q_{\min}^2, q_{\max}^2) = (1, 6), (2, 6), (1, 7), (2, 7)$ GeV² (from top to bottom). The uncertainties from the form factor $\xi_P(q^2)$ and the renormalization scale μ_b varied between $m_b/2$ and $2m_b$ are also given separately in percent of the central value. The corresponding branching ratios with electrons, \mathcal{B}_e , agree within uncertainties with the ones with muons, \mathcal{B}_μ . For details see text.

relations (A.3) and (A.4) we obtain a simple expression for F_H^l in the SM at low q^2 :

$$F_H^{l\text{SM}} = 2m_l^2 \frac{\Gamma_0}{\Gamma_l^{\text{SM}}} \int_{q_{\min}^2}^{q_{\max}^2} \frac{dq^2}{q^2} \xi_P^2(q^2) \sqrt{\lambda}^3 \beta_l (|F_A|^2 + |F_V|^2) \quad (5.2)$$

$$\times \left\{ 1 + \frac{q^2}{M_B^2} \times \mathcal{O} \left(\alpha_s, \frac{q^2}{M_B^2} \sqrt{\frac{\Lambda_{\text{QCD}}}{E}} \right) \right\},$$

where the denominator Γ_l^{SM} is given in (5.1). From the lepton mass suppression of $a_l + c_l$ in the numerator of (4.9) follows $F_H^{l\text{SM}} \propto m_l^2$, and $F_H^{e\text{SM}}/F_H^{\mu\text{SM}} \propto m_e^2/m_\mu^2$ such that $F_H^{e\text{SM}}$ is negligible. The cancellation between $a_\mu(q^2)$ and $c_\mu(q^2)$ is also visible from Figure 1 (left-hand plot). Note that the leading term of the integrand in the numerator of (5.2) is the same as the one in the denominator (5.1) except for an additional factor of $\beta_l/q^2 \simeq 1/q^2$. We therefore expect large cancellations of uncertainties in the ratio for low q^2 . This concerns the ones from the form factor, the renormalization scale, V_{ts} and unknown subleading $1/E$ corrections in \mathcal{T}_P .

As expected the SM values of F_H^μ are rather small, i.e., at the percent level, with the exact value depending on cuts. This can be seen from Figure 3, where F_H^μ is shown for $q_{\min}^2 = \{0.5, 1, 2\}$ GeV² versus the upper integration boundary q_{\max}^2 . For $q_{\min}^2 = \{1, 2\}$ GeV², F_H^μ ranges between 0.015 – 0.05 depending on the values of q_{\min}^2 and q_{\max}^2 .

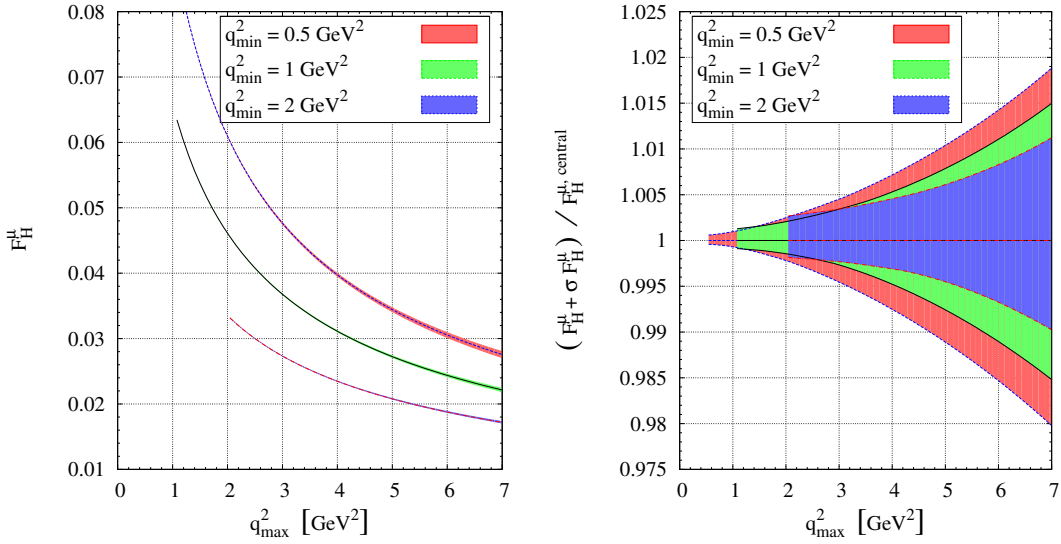


Figure 3: The observable F_H^μ in the SM depending on q_{\max}^2 for three cuts $q_{\min}^2 = \{0.5, 1, 2\}$ GeV² (left-hand plot) and normalized to the central value (right-hand plot). The bands include combined uncertainties from μ_b and the form factor $\xi_P(q^2)$.

F_H^μ becomes larger for smaller dilepton mass intervals and also for lower values of the lower cut q_{\min}^2 . SM values of F_H^μ are given for some low- q^2 cuts in Table 2. Within uncertainties, the predictions for $B^- \rightarrow K^- \bar{l}l$ and $\bar{B}^0 \rightarrow K^0 \bar{l}l$ decays are the same.

Indeed our numerical analysis of F_H^μ exhibits strong cancellations of uncertainties. The form factor ξ_P and μ_b induce uncertainties of comparable sizes of order one percent, see Table 2. The combined uncertainty from $\xi_P(q^2)$ and μ_b is indicated by the small bands in Figure 3 and result in an $\lesssim 2\%$ uncertainty, see also Table 2. Power counting suggests an additional uncertainty from form factor symmetry breaking of order $q^4/M_B^4 \sqrt{\Lambda_{\text{QCD}}/E} \sim 3\%$ in F_H^μ . We also allow for subleading power corrections to the hard scattering contributions at the order $q^2/M_B^2 \alpha_s \sqrt{\Lambda_{\text{QCD}}/E} \sim 3\%$, see Appendix A. Taking all this into account, F_H^μ can be predicted with an accuracy of $\sim \mathcal{O}(6\%)$ in the SM, which is a high precision for an observable in exclusive B -decays. Due to its huge suppression from m_e^2 , F_H^e is a null test of the SM. Comparing our SM predictions for R_K and F_H^μ , the former is known even more precisely due to the cancellation of the $\mathcal{O}(m_l^2)$ -terms at leading order in α_s and $1/E$ and the stronger suppression of the symmetry relation breaking corrections in Γ_l (5.1) compared to the ones in (5.2). In order for the relation (4.11) to hold, Δ^{SM} must be equal to $-F_H^{\mu \text{SM}}$ at the level of 10^{-4} .

As already mentioned in Section 4, operators in the effective theory of dimension higher than six or QED corrections induce additional contributions to the $\bar{B} \rightarrow K \bar{l}l$ decay amplitude, which can modify the angular distributions. As for the higher dimensional operators, in the SM they are, for example, generated at one-loop by the Higgs penguin and the box with one charged pseudo Goldstone- and one W -boson [30]. Contributions to scalar and pseudoscalar operators arise then at the order $C_{S,P}^{l \text{SM}} \sim m_l m_b / m_W^2$. Plugging

this into (3.2), (4.3) and (4.8), a non-zero forward-backward asymmetry $A_{\text{FB}}^{l\text{SM}} \sim m_l^2/m_W^2$ is induced, which is too small to be experimentally probed. The corresponding SM tensor contributions have not been calculated, but they are subject to a similar $\mathcal{O}(m_l m_b/m_W^2)$ suppression, and negligible as the scalar ones in the $\bar{B} \rightarrow K\bar{l}l$ observables.

Higher order α_e -corrections to exclusive $\bar{B} \rightarrow K\bar{l}l$ decays have not been considered so far. Besides reducing the uncertainty from the overall $\alpha_e(\mu)$ in the decay amplitude, radiative corrections can distort the decay distributions at the level of $\alpha_e/(4\pi)$. The generation of an interesting $\cos\theta$ -behavior from QED has been demonstrated for $K \rightarrow \pi e\bar{e}$ decays. Radiative corrections via $K \rightarrow \pi\gamma\gamma$ enter the $\bar{e}\gamma_\mu e$ -form factor in the matrix element, e.g., [31], which can be parametrized in our notation as $F_V \rightarrow F_V + \alpha_e/(4\pi) \cos\theta \tilde{F}_V$, see (3.1). Note that F_V, \tilde{F}_V are functions of q^2 only. The extra power of $\cos\theta$ implies not only a non-zero $A_{\text{FB}}^{l\text{SM}} \sim \alpha_e/(4\pi) \tilde{F}_V/C_9^{\text{SM}}$, but also a $\cos^3\theta$ -term of order $\alpha_e/(4\pi) \tilde{F}_V C_9^{\text{SM}}$ and a suppressed $\cos^4\theta$ -term of order $(\alpha_e/(4\pi) \tilde{F}_V)^2$ in the angular distributions. Unless the unknown correction factor \tilde{F}_V is significantly enhanced ($\gg 1$), it is unlikely that α_e -corrections have observable consequences in $\bar{B} \rightarrow K\bar{l}l$ decays.

6. Beyond the Standard Model

In the first part of this section we perform a model-independent analysis of $\bar{B} \rightarrow K\bar{l}l$ decays for $l = e$ and $l = \mu$. The size of the deviations from the SM in the observables F_H^l, R_K and A_{FB}^l due to the NP operators (2.3) is estimated. We show this for four benchmark scenarios in Section 6.1 to Section 6.4. The second part of this section, Section 6.5, contains a brief discussion of models with (pseudo-) scalar and tensor operators. All NP Wilson coefficients are assumed to be real and are understood to be at the low scale μ_b , i.e., here $C_i^l = C_i^l(\mu_b)$. Leading logarithmic renormalization group evolution to the electroweak scale can be done with the anomalous dimensions given in (2.4).

We start with some general considerations about the dependence of the $\bar{B} \rightarrow K\bar{l}l$ observables on the NP Wilson coefficients. Up to corrections of order m_l^3 we find for the branching ratio

$$\begin{aligned} \mathcal{B}_l = & \left[\frac{\tau_{B^\pm}}{1.64\text{ps}} \right] \left[1.91 + 0.02 (C_S^{l2} + C_P^{l2}) + 0.06 (C_T^{l2} + C_{T5}^{l2}) + \frac{m_l}{\text{GeV}} \left(\frac{C_T^l}{0.99} - \frac{C_P^l}{2.92} \right) \right. \\ & \left. + \frac{m_l^2}{\text{GeV}^2} \left(\frac{C_T^{l2}}{3.28^2} - \frac{C_{T5}^{l2}}{3.28^2} - \frac{C_P^{l2}}{10.36^2} - \frac{C_S^{l2}}{5.98^2} \right) + \mathcal{O}(m_l^3) \right] \cdot 10^{-7}, \end{aligned} \quad (6.1)$$

the numerator of F_H^l (4.9)

$$\begin{aligned} 2 \tau_{B^\pm} (A_l + C_l) = & \left[\frac{\tau_{B^\pm}}{1.64\text{ps}} \right] \left[\frac{m_l^2}{(0.51 \text{ GeV})^2} + 0.02 (C_S^{l2} + C_P^{l2}) + 0.19 (C_T^{l2} + C_{T5}^{l2}) \right. \\ & \left. + \frac{m_l}{\text{GeV}} \left(\frac{C_T^l}{0.99} - \frac{C_P^l}{2.92} \right) + \frac{m_l^2}{\text{GeV}^2} \left(\frac{C_T^{l2}}{3.28^2} - \frac{C_{T5}^{l2}}{1.89^2} - \frac{C_P^{l2}}{10.36^2} - \frac{C_S^{l2}}{5.98^2} \right) + \mathcal{O}(m_l^3) \right] \cdot 10^{-7}, \end{aligned} \quad (6.2)$$

and the numerator of the normalized forward-backward asymmetry (4.8)

$$\begin{aligned} \tau_{B^\pm} B_l = & \left[\frac{\tau_{B^\pm}}{1.64\text{ps}} \right] \left[0.06(C_S^l C_T^l + C_P^l C_{T5}^l) + \frac{m_l}{\text{GeV}} \left(\frac{C_S^l}{6.25} - \frac{C_{T5}^l}{1.85} \right) \right. \\ & \left. - \frac{m_l^2}{\text{GeV}^2} \left(\frac{C_S^l C_T^l}{4.12^2} + \frac{C_P^l C_{T5}^l}{4.12^2} \right) + \mathcal{O}(m_l^3) \right] \cdot 10^{-7}. \end{aligned} \quad (6.3)$$

Here, we integrated over the dilepton mass region $1 \text{ GeV}^2 < q^2 \leq 7 \text{ GeV}^2$ and used the central values of the input parameters given in Table 1. Then F_H^l is given by the ratio of (6.2) and (6.1), R_K by the ratio of (6.1) for $l = \mu$ and $l = e$ and A_{FB}^l by the ratio of (6.3) and (6.1), respectively. The contributions of the chirality flipped operators $\mathcal{O}_{S,P}^l$ can be included by the replacement $C_{S,P}^l \rightarrow C_{S,P}^l + C_{S,P}^{\prime l}$.

As can be seen from (6.1), the $\bar{B} \rightarrow K \bar{l} l$ branching ratio is not very sensitive to NP effects from scalar and tensor operators due to the small coefficients in front of the NP couplings with respect to the large SM contribution. Moreover, the SM uncertainties of \mathcal{B}_l will hide NP unless the Wilson coefficients become large, $C_i^{\text{NP}} \gtrsim 1$. This actually can happen in some NP scenarios as we will show, in particular, in the decays into electrons, where the current experimental constraints are looser than the ones for the muons. Due to its tiny theory uncertainty the ratio R_K is a much more powerful probe of NP than the $\bar{B} \rightarrow K \bar{l} l$ branching ratios. Especially the terms at zeroth order in the lepton mass but also the ones linear in m_μ can significantly modify $R_K - 1$ with respect to its negligible SM value.

The angular observables F_H^l (6.2) and A_{FB}^l (6.3) share several features with $R_K - 1$: They have a small and clean SM prediction and the sensitivity to tensor operators is higher than to scalar and pseudoscalar ones. Note that the dependence of \mathcal{B}_l and F_H^l on the (pseudo-) scalar Wilson coefficients is the same and that the leading term in the lepton-mass expansion of A_{FB}^l requires the presence of both (pseudo-) scalar and tensor operators. Note also that R_K can be affected independently by NP in $\bar{B} \rightarrow K \bar{e} e$ and $\bar{B} \rightarrow K \bar{\mu} \mu$ decays.

The available experimental information on F_H^l , $R_K - 1$ and A_{FB}^l including SM predictions is given in Table 3 together with other related $b \rightarrow s \bar{l} l$ decay observables. The data on R_K include large dilepton masses where QCDF is not applicable and the ones on F_H^l and A_{FB}^l are in addition lepton flavor averaged. We do not take these constraints into account since they cannot be applied in a straightforward way besides having sizeable uncertainties.

Important constraints on NP come from $\mathcal{B}(\bar{B}_s \rightarrow \bar{l} l)$, which can be written as

$$\begin{aligned} \mathcal{B}(\bar{B}_s \rightarrow \bar{l} l) = & \frac{G_F^2 \alpha_e^2 M_{B_s}^5 f_{B_s}^2 \tau_{B_s}}{64\pi^3} |V_{tb} V_{ts}^*|^2 \sqrt{1 - \frac{4m_l^2}{M_{B_s}^2}} \\ & \times \left\{ \left(1 - \frac{4m_l^2}{M_{B_s}^2} \right) \left| \frac{C_S^l - C_S^{\prime l}}{m_b + m_s} \right|^2 + \left| \frac{C_P^l - C_P^{\prime l}}{m_b + m_s} + \frac{2m_l}{M_{B_s}^2} C_{10} \right|^2 \right\}. \end{aligned} \quad (6.4)$$

The $\bar{B}_s \rightarrow \bar{l} l$ branching ratios depend on the difference of Wilson coefficients ($C_{S,P}^l - C_{S,P}^{\prime l}$). It follows that constraints from (6.4) can be evaded in the presence of both unprimed and primed (pseudo-) scalar Wilson coefficients unless there is a complementary constraint

observable	sensitive to	SM value	data
F_H^μ	$C_{S,P}^\mu + C_{S,P}^{\mu'}$, $C_{T(5)}^\mu$	$\mathcal{O}(m_\mu^2/q^2)$	$0.81_{-0.61}^{+0.58} \pm 0.46^\dagger$ [4]
A_{FB}^μ	$C_{S,P}^\mu + C_{S,P}^{\mu'}$, $C_{T(5)}^\mu$	$\mathcal{O}(\alpha_e/(4\pi))$	$0.15_{-0.23}^{+0.21} \pm 0.08^\dagger$ [4] $0.10 \pm 0.14 \pm 0.01^\dagger$ [3]
$R_K - 1$	$C_{S,P}^l + C_{S,P}^{l'}$, $C_{T(5)}^l$, e vs. μ	$\mathcal{O}(10^{-4})$	$0.24 \pm 0.31^\dagger$ [2, 4]
$\mathcal{B}(\bar{B}_s \rightarrow \bar{\mu}\mu)$	$C_{S,P}^\mu - C_{S,P}^{\mu'}$	$(3.23 \pm 0.44) \cdot 10^{-9}$	$< 8.0 \cdot 10^{-8}$ [5]
$\mathcal{B}(\bar{B}_s \rightarrow \bar{e}e)$	$C_{S,P}^e - C_{S,P}^{e'}$	$(7.56 \pm 0.32) \cdot 10^{-14}$	$< 5.4 \cdot 10^{-5}$ [33]
$\mathcal{B}_\mu^{\text{incl}} _{>0.04}$	$C_S^{\mu(l)} \pm C_P^{\mu(l)}$, $C_{T(5)}^\mu$	$(4.15 \pm 0.70) \cdot 10^{-6}$ [6]	$(4.3 \pm 1.2) \cdot 10^{-6}$ [20]
$\mathcal{B}_e^{\text{incl}} _{>0.04}$	$C_S^{e(l)} \pm C_P^{e(l)}$, $C_{T(5)}^e$	$(4.15 \pm 0.70) \cdot 10^{-6}$ [6]	$(4.7 \pm 1.3) \cdot 10^{-6}$ [20]

Table 3: Observables in $b \rightarrow s\bar{l}l$ induced transitions. Upper bounds are given at 90% C.L. For details see text. † Data include q^2 -regions where QCDF does not apply and both $l = e$ and μ are included.

such as on $(C_{S,P}^l + C_{S,P}^{l'})$ from $\bar{B} \rightarrow K\bar{l}l$ decays [8]. Tensor operators do not contribute to $\bar{B}_s \rightarrow \bar{l}l$ decays and hence $C_{T,T5}^l$ are not constrained by these decays. The current 90% C.L. upper bound on $\mathcal{B}(\bar{B}_s \rightarrow \bar{l}l)$ for $l = \mu$ comes from CDF and DØ [5]¹ and for electrons from L3 [33]. The experimental information can be seen in Table 3 together with the SM predictions obtained with the input from Table 1. The bound on $\mathcal{B}(\bar{B}_s \rightarrow \bar{\mu}\mu)$ is $\mathcal{O}(20)$ away from the SM, and the one for electrons is nine orders of magnitude above the SM. As we show in Section 6.1, the current $\mathcal{B}(\bar{B}_s \rightarrow \bar{e}e)$ constraint is nevertheless on the verge of being useful, since NP in $C_{S,P}^{l(l)}$ does not enter the $\bar{B}_s \rightarrow \bar{l}l$ modes with m_l -suppression as the SM contribution, see (6.4).

We further take into account the measurements of the branching ratios of the inclusive $\bar{B} \rightarrow X_s \bar{e}e$ and $\bar{B} \rightarrow X_s \bar{\mu}\mu$ decays for $q^2 > 0.04 \text{ GeV}^2$ denoted by $\mathcal{B}_l^{\text{incl}}|_{>0.04}$. The corresponding experimental values [20, 34] can be seen in Table 3 with SM predictions from [6]. The q^2 -cut dependent $\bar{B} \rightarrow X_s \bar{l}l$ branching ratios with (pseudo-) scalar and tensor interactions can be written as (see, e.g., [35])

$$\begin{aligned} \mathcal{B}_l^{\text{incl}}|_{[q_{\text{min}}^2, q_{\text{max}}^2]} \equiv \mathcal{B}(\bar{B} \rightarrow X_s \bar{l}l) &= \mathcal{B}_l^{\text{incl}}|_{[q_{\text{min}}^2, q_{\text{max}}^2], \text{SM}} + (|C_T^l|^2 + |C_{T5}^l|^2) \mathcal{M}_T \\ &+ (|C_S^l + C_P^l|^2 + |C_S^{l'} + C_P^{l'}|^2 + |C_S^l - C_P^l|^2 + |C_S^{l'} - C_P^{l'}|^2) \mathcal{M}_S, \end{aligned} \quad (6.5)$$

where

$$\mathcal{M}_{S,T} = \frac{\mathcal{B}_0}{2m_b^8} \int_{q_{\text{min}}^2}^{q_{\text{max}}^2} dq^2 M_{S,T}(q^2), \quad \mathcal{B}_0 = \frac{3\alpha_e^2}{(4\pi)^2} \frac{|V_{tb}V_{ts}^*|^2}{|V_{cb}|^2} \frac{\mathcal{B}(\bar{B} \rightarrow X_c l \bar{\nu}_l)}{f(m_c/m_b)\kappa(m_c/m_b)} \quad (6.6)$$

and

$$M_S(q^2) = 2q^2(m_b^2 - q^2)^2, \quad M_T(q^2) = \frac{64}{3}(m_b^2 - q^2)^2(2m_b^2 + q^2). \quad (6.7)$$

¹A stronger bound has been reported from a combined CDF and DØ analysis at 95% C.L., $\mathcal{B}(\bar{B}_s \rightarrow \bar{\mu}\mu) < 5.8 \cdot 10^{-8}$ [32].

Here we neglect kinematical factors of m_s and m_l in the NP part and evaluate (6.6) and (6.7) with a b -quark mass of 4.8 GeV, corresponding to the pole mass in accordance with [6]. The functions $f(m_c/m_b)$ and $\kappa(m_c/m_b)$ represent the phase space function and QCD corrections of the decay $\bar{B} \rightarrow X_c l \bar{\nu}_l$, respectively, and can be seen in [35]. Since $M_{S,T} > 0$, NP from (pseudo-) scalar and tensor contributions enhances the $\bar{B} \rightarrow X_s \bar{l} l$ branching ratios, and only the upper boundary of the experimental value of $\mathcal{B}(\bar{B} \rightarrow X_s \bar{l} l)$ becomes a constraint on the corresponding Wilson coefficients. Also, since $M_T \gg M_S$, the inclusive branching ratios are more sensitive to tensor than scalar and pseudoscalar operators. Numerically, for $0.04 \text{ GeV}^2 < q^2 \leq m_b^2$ we obtain $\mathcal{M}_S = 1.92 \cdot 10^{-8}$ and $\mathcal{M}_T = 1.84 \cdot 10^{-6}$.

In our NP analysis we also predict $\mathcal{B}_l^{\text{incl}}|_{[1,6]}$ for $l = e, \mu$ using $\mathcal{B}_e^{\text{incl}}|_{[1,6],\text{SM}} = (1.64 \pm 0.11) \cdot 10^{-6}$ and $\mathcal{B}_\mu^{\text{incl}}|_{[1,6],\text{SM}} = (1.59 \pm 0.11) \cdot 10^{-6}$ [29]. These values are close to the experimental world average $\mathcal{B}_l^{\text{incl}}|_{[1,6],\text{exp}} = (1.60 \pm 0.51) \cdot 10^{-6}$ [34] which is lepton flavor averaged and we therefore do not consider it as a constraint. However, we use this to illustrate the physics potential of future lepton flavor specific $\mathcal{B}_e^{\text{incl}}|_{[1,6]}$ and $\mathcal{B}_\mu^{\text{incl}}|_{[1,6]}$ measurements. The $\mathcal{M}_{S,T}$ -coefficients for this low dilepton mass region $1 \text{ GeV}^2 < q^2 \leq 6 \text{ GeV}^2$ are $\mathcal{M}_S = 0.52 \cdot 10^{-8}$ and $\mathcal{M}_T = 0.83 \cdot 10^{-6}$. Note that we used here the b -quark pole mass in the NP part of $\mathcal{B}(\bar{B} \rightarrow X_s \bar{l} l)$ as well. To be consistent with the SM results of [29] the 1S mass should be used once the next-to-leading order corrections to the NP part are known.

Given the existing experimental constraints we cannot perform at present a fully model-independent analysis and fit for the six real NP Wilson coefficients per lepton species. Instead, we entertain in the following four benchmark scenarios with (pseudo-) scalar operators (Scenario I-III) and the tensor operators (Scenario IV) defined as:

- Scenario I: NP in C_S^l and C_P^l , all other NP contributions vanish.
- Scenario II: Same as Scenario I, but with the additional assumptions $C_S^l = -C_P^l$ and $C^l \propto m_l$.
- Scenario III: NP in C_S^l, C_P^l and C_S^l, C_P^l , the tensor coefficients $C_{T,T5}^l$ vanish.
- Scenario IV: NP in the tensor coefficients C_T^l, C_{T5}^l , all other NP contributions vanish.

Scenario II is inspired by the Minimal Supersymmetric Standard Model (MSSM) for large values of $\tan \beta$, where $\tan \beta$ denotes the ratio of the two Higgs vacuum expectation values, see also Section 6.5.

All $\bar{B} \rightarrow K \bar{l} l$ observables are obtained for $1 \text{ GeV}^2 < q^2 \leq 7 \text{ GeV}^2$. We employ all bounds at 90% C.L. The resulting allowed ranges of the NP Wilson coefficients and the $b \rightarrow s \bar{l} l$ decay observables are summarized in Table 4 and Table 5, respectively. Since the current experimental errors dominate the uncertainties, in the following we do not take into account SM uncertainties. Their inclusion would allow for slightly bigger NP effects.

6.1 Scenario I: Scalars C_S^l and C_P^l

We start with a discussion of the Wilson coefficients for muons, $C_{S,P}^\mu$. The bounds on $C_{S,P}^\mu$ from (6.4) are displayed in the left hand plot of Figure 4, where contours of $\mathcal{B}(\bar{B}_s \rightarrow \bar{\mu} \mu) < \{0.05, 0.1, 0.2, 0.4, 0.6, 0.8, 1.0\} \cdot 10^{-7}$ are shown. The ranges for $C_{S,P}^\mu$ after applying the 90%

Wilson coefficient	Sc I	Sc II	Sc III	Sc IV
$C_{S,P}^e$	$[-8.3, 8.3]$	–	$[-8.3, 8.3]$	–
C_S^μ	$[-0.69, 0.69]$	$[-0.55, 0.41]$	$[-5.6, 5.6]$	–
C_P^μ	$[-0.55, 0.82]$	$= -C_S^\mu$	$[-5.6, 5.6]$	–
$C_{S,P}^{e'}$	–	–	$[-8.3, 8.3]$	–
$C_{S,P}^{\mu'}$	–	–	$[-5.6, 5.6]$	–
$C_{T,T5}^e$	–	–	–	$[-1.2, 1.2]$
$C_{T,T5}^\mu$	–	–	–	$[-1.1, 1.1]$

Table 4: The allowed ranges for the NP Wilson coefficients C_i^l in Scenarios I-IV after using the constraints $\mathcal{B}(\bar{B}_s \rightarrow \bar{e}e) < 5.4 \cdot 10^{-5}$, $\mathcal{B}(\bar{B}_s \rightarrow \bar{\mu}\mu) < 0.8 \cdot 10^{-7}$, $\mathcal{B}_e^{\text{incl}}|_{>0.04} < 6.8 \cdot 10^{-6}$ and $\mathcal{B}_\mu^{\text{incl}}|_{>0.04} < 6.3 \cdot 10^{-6}$, see Table 3. A “–” means that the corresponding coefficient is zero in this NP scenario.

C.L. $\mathcal{B}(\bar{B}_s \rightarrow \bar{\mu}\mu)$ upper bound given in Table 3 can be seen in Table 4. The corresponding ranges of the observables are presented in Table 5. As can be seen, F_H^μ can deviate from the SM by about 40% whereas the forward-backward asymmetry is less than 1% in agreement with and updating earlier findings [7]. The deviation of the branching ratio \mathcal{B}_μ from the SM is less than 2% and completely negligible in view of the theoretical uncertainties. Also the NP contributions to $\mathcal{B}_\mu^{\text{incl}}|_{[1,6]}$ and $\mathcal{B}_\mu^{\text{incl}}|_{>0.04}$ are small compared to the theoretical uncertainties.

The situation for the electrons is different due to the weaker bound from $\mathcal{B}(\bar{B}_s \rightarrow \bar{e}e)$ such that $\mathcal{B}_e^{\text{incl}}|_{>0.04}$ gives the strongest constraint on $C_{S,P}^e$. In the right-hand plot of Figure 4 contours in the $C_S^e - C_P^e$ plane are shown for $\mathcal{B}_e^{\text{incl}}|_{>0.04} < \{4.5, 5.0, 6.0, 6.8, 8.0\} \cdot 10^{-6}$ and $\mathcal{B}(\bar{B}_s \rightarrow \bar{e}e) < \{0.1, 0.5, 1.0\} \cdot 10^{-5}$. The latter illustrates the constraints of improved measurements of $\mathcal{B}(\bar{B}_s \rightarrow \bar{e}e)$. We encounter the large ranges of $C_{S,P}^e$ given in Table 4 allowed by $\mathcal{B}_e^{\text{incl}}|_{>0.04} < 6.8 \cdot 10^{-6}$ at 90% C.L., see Table 3. The corresponding ranges for the decay observables for $l = e$ are presented in Table 5. As one can see, F_H^e can be enhanced by orders of magnitude compared to its negligible SM value. Furthermore, F_H^e is strongly correlated to \mathcal{B}_e , R_K (see (6.1) and (6.2)) and $\mathcal{B}_e^{\text{incl}}|_{[1,6]}$. The observables F_H^e , \mathcal{B}_e and $\mathcal{B}_e^{\text{incl}}|_{[1,6]}$ increase for increasing $|C_{S,P}^e|$ whereas R_K decreases. We show \mathcal{B}_e versus F_H^e (left-hand plot) and R_K versus F_H^e (right-hand plot) in Figure 5. The branching ratio \mathcal{B}_e can be enhanced by about 60% with respect to its SM value. $\mathcal{B}_e^{\text{incl}}|_{[1,6]}$ exhibits a similar enhancement but is subject to smaller theoretical uncertainties. The forward-backward asymmetry A_{FB}^e is negligibly small.

The observable R_K depends on both lepton channels $l = e, \mu$. In Scenario I the denominator \mathcal{B}_e receives large NP contributions whereas the numerator \mathcal{B}_μ stays close to its SM value due to the strong constraint from $\bar{B}_s \rightarrow \bar{\mu}\mu$. This leads to a substantial decrease of R_K with respect to the SM as can be seen in Table 5 and also in the right-hand plot of Figure 5.

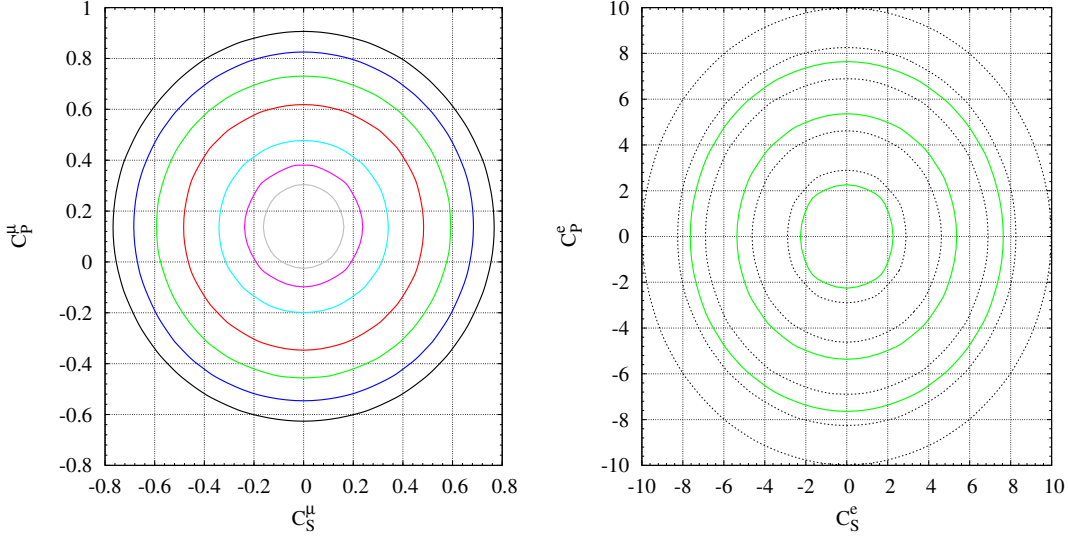


Figure 4: In the left-hand plot contours of $\mathcal{B}(\bar{B}_s \rightarrow \bar{\mu}\mu)$ are shown in the $C_S^\mu - C_P^\mu$ plane in Scenario I. The contours enclose values of $\mathcal{B}(\bar{B}_s \rightarrow \bar{\mu}\mu) < \{0.05, 0.1, 0.2, 0.4, 0.6, 0.8, 1.0\} \cdot 10^{-7}$ starting with the innermost. In the right-hand plot contours of $\mathcal{B}_e^{\text{incl}}|_{>0.04} < \{4.5, 5.0, 6.0, 6.8, 8.0\} \cdot 10^{-6}$ (dashed black) and $\mathcal{B}(\bar{B}_s \rightarrow \bar{e}e) < \{0.1, 0.5, 1.0\} \cdot 10^{-5}$ (solid green) are shown in the $C_S^e - C_P^e$ plane in Scenario I starting with the innermost.

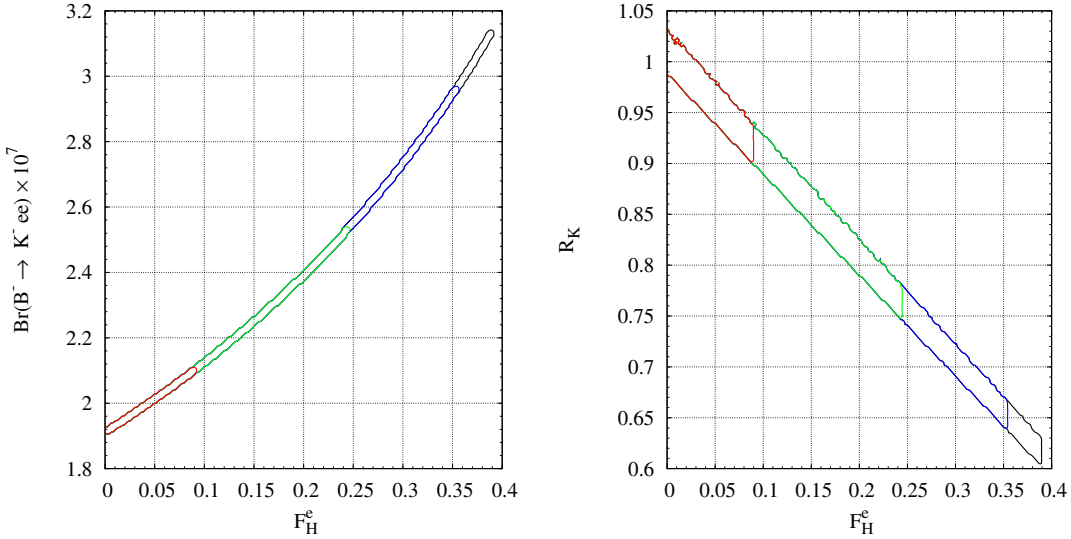


Figure 5: Contours of $\mathcal{B}_e^{\text{incl}}|_{[1,6]} < \{1.75, 2.0, 2.25, 2.35\} \cdot 10^{-6}$ in the $F_H^e - \mathcal{B}_e$ plane (left-hand plot) and the $F_H^e - R_K$ plane (right-hand plot) in Scenario I.

6.2 Scenario II: MSSM-like $C_S^\mu = -C_P^\mu$

Scenario II is a special case of Scenario I inspired by the MSSM in a certain limit (large

Observable	Sc I	Sc II	Sc III	Sc IV
F_H^e	< 0.39	–	< 0.56	< 0.13
F_H^μ	[0.013, 0.035]	[0.018, 0.032]	[0.013, 0.56]	[0.014, 0.18]
R_K	[0.61, 1.01]	[0.996, 1.01]	[0.44, 2.21]	[0.93, 1.10]
$\mathcal{B}_e [10^{-7}]$	[1.91, 3.14]	–	[1.91, 4.36]	[1.91, 2.00]
$\mathcal{B}_\mu [10^{-7}]$	[1.90, 1.94]	[1.90, 1.93]	[1.90, 4.26]	[1.87, 2.10]
$A_{\text{FB}}^e [\%]$	[−0.02, 0.02]	–	[−0.02, 0.02]	[−0.02, 0.02]
$A_{\text{FB}}^\mu [\%]$	[−0.6, 0.6]	[−0.5, 0.3]	[−4.46, 4.46]	[−3.1, 3.1]
$\mathcal{B}(\bar{B}_s \rightarrow \bar{e}e) [10^{-5}]$	< 1.17	–	< 2.33	–
$\mathcal{B}(\bar{B}_s \rightarrow \bar{\mu}\mu) [10^{-7}]$	< 0.8	< 0.8	< 0.8	–
$\mathcal{B}_e^{\text{incl}} _{[1,6]} [10^{-6}]$	[1.64, 2.35]	–	[1.64, 2.35]	[1.64, 2.83]
$\mathcal{B}_\mu^{\text{incl}} _{[1,6]} [10^{-6}]$	[1.59, 1.60]	[1.59, 1.60]	[1.59, 2.17]	[1.59, 2.56]
$\mathcal{B}_e^{\text{incl}} _{>0.04} [10^{-6}]$	[4.15, 6.8]	–	[4.15, 6.8]	[4.15, 6.8]
$\mathcal{B}_\mu^{\text{incl}} _{>0.04} [10^{-6}]$	[4.15, 4.18]	[4.15, 4.17]	[4.15, 6.3]	[4.15, 6.3]

Table 5: Allowed ranges for $b \rightarrow s\bar{l}l$ observables in Scenarios I-IV after taking into account the constraints from $\mathcal{B}(\bar{B}_s \rightarrow \bar{l}l)$ and $\mathcal{B}_l^{\text{incl}}|_{>0.04}$ for $l = e$ and $l = \mu$, see Table 3 and the text for details. A “–” means that the corresponding observable is SM-like.

$\tan\beta$), see also Section 6.5. In this model, the (pseudo-) scalar Wilson coefficients are proportional to the lepton mass $C_{S,P}^l \sim m_l$, such that $C_{S,P}^e$ can be neglected and $b \rightarrow s\bar{e}e$ decays are SM-like. Furthermore the relation $C_S^\mu = -C_P^\mu$ holds and the primed coefficients $C_{S,P}^{\mu'}$ are suppressed by m_s/m_b and can be neglected.

The allowed range of C_S^μ and the effects of NP on the rare decay observables are given in Table 4 and Table 5, respectively. Since Scenario II is a constrained variant of Scenario I the deviations from the SM are smaller in the former. The NP contributions to F_H^μ do not exceed 30% whereas the deviations of \mathcal{B}_μ from the SM are of the order of 2%, much smaller than the theoretical uncertainties. The same holds for $\mathcal{B}_\mu^{\text{incl}}|_{[1,6]}$, which confirms earlier studies within the MSSM [36]. Since \mathcal{B}_e is SM-like in Scenario II, the deviation of R_K from the SM is much reduced with respect to the one in Scenario I. We find NP effects of 1%, which are larger than the uncertainties of the SM prediction. The forward-backward asymmetry is smaller than 1% in agreement with previous works in the framework of the MSSM [37].

6.3 Scenario III: Scalars C_S^l, C_P^l and $C_S^{\prime l}, C_P^{\prime l}$

In Scenario III we use the full set of (pseudo-) scalar Wilson coefficients including the chirality flipped ones $C_{S,P}^{\prime l}$ for $l = e$ and $l = \mu$. The constraint from the $\bar{B}_s \rightarrow \bar{l}l$ branching ratios alone can be evaded due to cancellations between $C_{S,P}^l$ and $C_{S,P}^{\prime l}$, see (6.4). To obtain constraints on $C_{S,P}^{\prime l}$ we combine $\mathcal{B}(\bar{B}_s \rightarrow \bar{l}l)$ with $\mathcal{B}_l^{\text{incl}}|_{>0.04}$ data. We find the allowed ranges for the Wilson coefficients given in Table 4. In the electron sector $C_{S,P}^e$ can

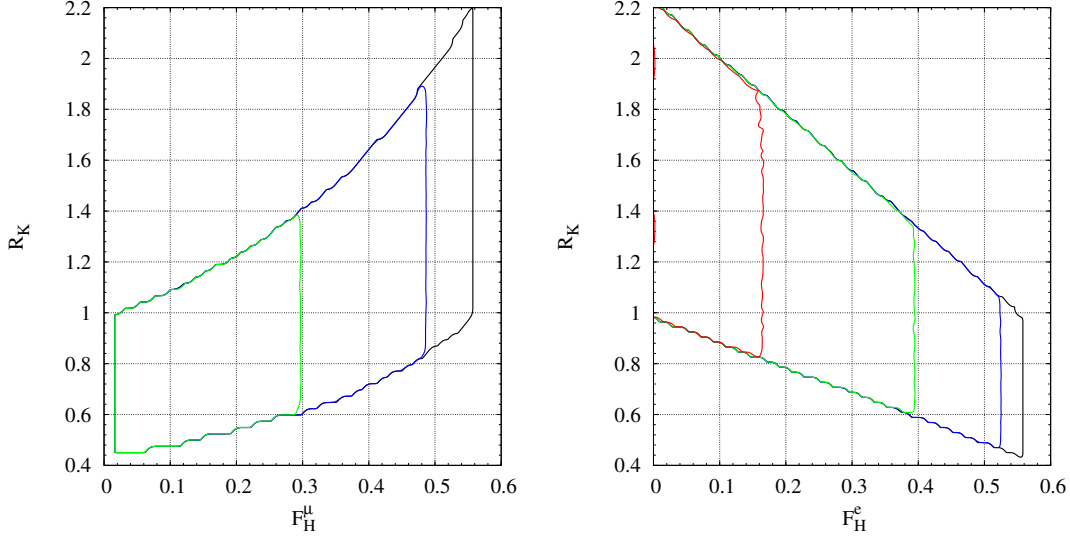


Figure 6: Contours of $\mathcal{B}_\mu^{\text{incl}}|_{[1,6]} < \{1.75, 2.0, 2.17\} \cdot 10^{-6}$ in the $F_H^\mu - R_K$ plane in Scenario III (left-hand plot). In the right-hand plot contours of $\mathcal{B}_e^{\text{incl}}|_{[1,6]} < \{1.75, 2.0, 2.25, 2.35\} \cdot 10^{-6}$ are shown in the $F_H^e - R_K$ plane in Scenario III. For details see text.

be as big as in Scenario I with identical ranges for $C_{S,P}^{e\prime}$. In the muon sector the Wilson coefficients $C_{S,P}^{\mu(l)}$ are now comparable in magnitude to the ones for electrons.

The large Wilson coefficients lead to big NP effects in the rare decay observables, see Table 5. In Scenario III R_K can both increase and decrease significantly with respect to the SM as opposed to Scenario I where $\mathcal{B}(\bar{B}_s \rightarrow \bar{\mu}\mu)$ permits only a large decrease of R_K . The substantial deviations of R_K from the SM are already challenged by existing data given in Table 3. However, as already stressed, since these data contain also large- q^2 events where QCDF is not applicable it is not clear how to impose these constraints in a well-defined way.

The increase of both F_H^μ and R_K for increasing values of $\mathcal{B}_\mu^{\text{incl}}|_{[1,6]}$ can be seen in the left-hand plot of Figure 6, where contours of $\mathcal{B}_\mu^{\text{incl}}|_{[1,6]} < \{1.75, 2.0, 2.17\} \cdot 10^{-6}$ are shown. Similarly, the increase of F_H^e and decrease of R_K for increasing values of $\mathcal{B}_e^{\text{incl}}|_{[1,6]}$ is displayed in the right-hand plot of Figure 6 with contours of $\mathcal{B}_e^{\text{incl}}|_{[1,6]} < \{1.75, 2.0, 2.25, 2.35\} \cdot 10^{-6}$. The NP contributions enhance both \mathcal{B}_e and \mathcal{B}_μ by order 200% above the SM such that measurements of these observables in the low- q^2 region could provide constraints regardless of the large form factor uncertainties. Scenario III allows for $|A_{\text{FB}}^\mu| \lesssim (4 - 5)\%$ whereas A_{FB}^e is negligibly small.

6.4 Scenario IV: Tensors C_T^l, C_{T5}^l

In Scenario IV we consider only NP in $C_{T,T5}^l$. These Wilson coefficients do not contribute to $\bar{B}_s \rightarrow \bar{l}l$ decays and hence are currently constrained only by inclusive $\bar{B} \rightarrow X_s \bar{l}l$ decays (6.5). The corresponding bounds can be seen in the left-hand plot of Figure 7, where contours of $\mathcal{B}_e^{\text{incl}}|_{>[0.04]} < \{4.5, 5.5, 6.3, 6.8, 8.0\} \cdot 10^{-6}$ are shown in the $C_T^e - C_{T5}^e$ plane

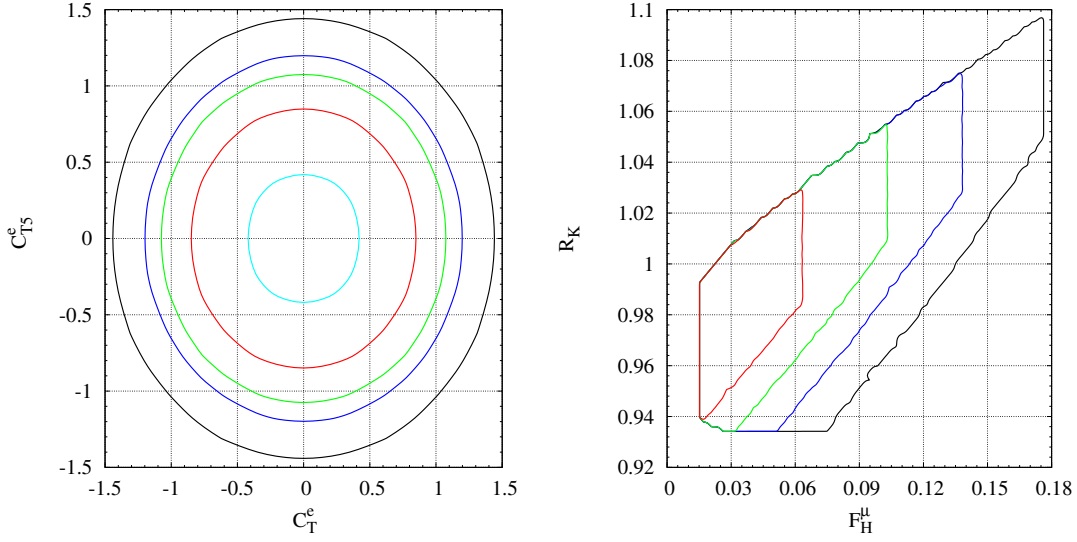


Figure 7: In the left-hand plot contours of $\mathcal{B}_e^{\text{incl}}|_{>0.04}$ are shown in the $C_T^e - C_{T5}^e$ plane in Scenario IV. Each contour encloses values of $\mathcal{B}_e^{\text{incl}}|_{>0.04} < \{4.5, 5.5, 6.3, 6.8, 8.0\} \cdot 10^{-6}$ starting with the innermost. Corresponding constraints for $C_T^\mu - C_{T5}^\mu$ can be read off from the left-hand plot as well. In the right-hand plot contours of $\mathcal{B}_\mu^{\text{incl}}|_{[1,6]} < \{1.75, 2.0, 2.25, 2.56\} \cdot 10^{-6}$ are shown for F_H^μ versus R_K in Scenario IV starting with the innermost.

starting with the innermost. The constraints on $C_{T,T5}^\mu$ from upper bounds on $\mathcal{B}_\mu^{\text{incl}}|_{>0.04}$ can be read off from the same plot. We find the ranges of the Wilson coefficients given in Table 4 using the 90% C.L. constraints $\mathcal{B}_e^{\text{incl}}|_{>0.04} < 6.8 \cdot 10^{-6}$ and $\mathcal{B}_e^{\text{incl}}|_{>0.04} < 6.3 \cdot 10^{-6}$, see Table 3. As anticipated after (6.7), $\mathcal{B}_l^{\text{incl}}|_{>0.04}$ constrains $C_{T,T5}^l$ stronger than $C_{S,P}^{l(i)}$.

The NP effects in F_H^e and F_H^μ are huge with respect to the SM predictions as can be seen in Table 5. F_H^l increases for increasing $\mathcal{B}_l^{\text{incl}}|_{[1,6]}$. This correlation is shown in the right-hand plot of Figure 7 for contours of $\mathcal{B}_\mu^{\text{incl}}|_{[1,6]} < \{1.75, 2.0, 2.25, 2.56\} \cdot 10^{-6}$ in the $F_H^\mu - R_K$ plane. Similar correlations hold for the electron sector. R_K receives order 10% corrections from NP which are well above the theoretical uncertainties. The branching ratios \mathcal{B}_l are subject to NP contributions $\lesssim +10\%$, which cannot be separated from the larger form factor induced uncertainties. On the other hand, the NP enhancements due to $C_{T,T5}^l$ in $\mathcal{B}_l^{\text{incl}}|_{[1,6]}$ are larger, about 70%, which makes the inclusive decays a sensitive probe of tensor operators. As in all other Scenarios I-III A_{FB}^e is negligibly small. $|A_{\text{FB}}^\mu|$ does not exceed 3%.

6.5 Models with Scalar and Tensor Interactions

While there are several known models beyond the SM with large (pseudo-) scalar interactions, tensor operators are often neglected. Let us begin with some general remarks on the origin of $b \rightarrow s\bar{l}l$ tensor operators in the SM and the MSSM: In the SM they arise only at higher order in the electroweak operator product expansion (OPE) from finite external momenta in the matching calculation. In the MSSM tensor operators are induced at

leading order OPE only from photino and zino box diagrams, which are, however, subleading in $\tan\beta$ with respect to the Higgs penguins discussed below. Higgsino contributions to tensors are further suppressed by down-type quark and lepton Yukawa couplings [38]. In addition tensors with two leptons are induced by scalar operators under QED renormalization group running, hence are of higher order in $\alpha_e/(4\pi) \cdot \log(\mu/\mu_b)$, e.g., [8, 14]. Another mechanism to generate tensor contributions is to consider models with scalars having appropriate quantum numbers such that tree level exchange induces the operators $(\bar{l}_L b_R)(\bar{s}_L l_R)$ or $(\bar{l}_R b_L)(\bar{s}_R l_L)$. Subsequent fierzing then leads to tensor operators. Among this class of models are those with leptoquarks. We consider such models below after briefly commenting on the MSSM at large $\tan\beta$ and the MSSM with broken R -parity.

For large values of $\tan\beta$ the MSSM produces substantial scalar couplings $C_{S,P}^l$ from Higgs penguins, for example, induced by chargino loops

$$C_{S,P}^l \propto \frac{m_l m_b}{m_{A^0}^2} \tan^3 \beta, \quad C_{S,P}^{\prime l} \simeq \frac{m_s}{m_b} C_{S,P}^l, \quad (6.8)$$

for exact Wilson coefficients see [7]. Here, m_{A^0} denotes the mass of the pseudoscalar Higgs boson. The relation $C_S^l = -C_P^l$ holds only at leading order in $\tan\beta$ [7] and prevents the generation of tensor couplings from QED running [8]. The flipped coefficients $C_{S,P}^{\prime l}$ are suppressed by the mass of the strange quark. Since $C^l \propto m_l$ the couplings to electrons are negligible.

In R -parity violating supersymmetry scalar and pseudoscalar FCNC-operators can be generated at tree level from the superpotential (see, e.g., [39])

$$W_R = \lambda_{ijk} L_L^i L_L^j \bar{e}_R^k + \lambda'_{ijk} L_L^i Q_L^j \bar{d}_R^k, \quad (6.9)$$

where $L_L(Q_L)$ and $e_R(d_R)$ denote the superfields containing the lepton (quark) doublet and the charged lepton (down-type quark) singlet, respectively. One gets at the matching scale from sneutrino exchange

$$C_{S,P}^l \propto \frac{(4\pi)^2}{e^2} \frac{\lambda_{k23}^* \lambda_{kll}}{V_{tb} V_{ts}^* G_F m_{\tilde{\nu}_k}^2}, \quad C_{S,P}^{\prime l} \propto \frac{(4\pi)^2}{e^2} \frac{\lambda'_{k32} \lambda_{kll}^*}{V_{tb} V_{ts}^* G_F m_{\tilde{\nu}_k}^2}. \quad (6.10)$$

Here $m_{\tilde{\nu}}$ denotes the sneutrino mass and summation over the sneutrino flavor k is understood. Contributions from squark exchange modify only the vector and axial vector type operators and are not shown. The couplings in (6.10) obey $C_S^l = -C_P^l$ and $C_S^{\prime l} = +C_P^{\prime l}$. As in the MSSM at large $\tan\beta$ with unbroken R -parity discussed previously, there are no tensor operators generated from leading order matching. The chirality flipped contributions can be sizeable and help to escape the constraint from $\bar{B}_s \rightarrow \bar{l}l$. The couplings (6.10) are then essentially only constrained by the $\bar{B} \rightarrow (K^{(*)}, X_s) \bar{e}e$ and $\bar{B} \rightarrow (K^{(*)}, X_s) \bar{\mu}\mu$ branching ratios. The size of the possible modification of R_K from one is then given by the theoretical and experimental uncertainties of the branching ratios, see also [40].

The Lagrangian of leptoquarks ϕ_{LQ} coupling to a lepton and a quark can be written as

$$\mathcal{L}_{LQ-l-q} = \lambda_{ij} l_i^l q_j \phi_{LQ}, \quad (6.11)$$

where i, j label the lepton and quark generation, respectively. ϕ_{LQ} can be a scalar or a vector under space-time transformations and a singlet, doublet or triplet under $SU(2)$. Details can be seen, e.g., in [41], where also contributions to flavor-changing scalar and pseudoscalar operators have been discussed. Here we consider only the contributions to tensor operators, which are induced by tree level scalar leptoquark exchange and fierzing as explained earlier. The $SU(2)$ -properties of the requisite operators require mixing of leptoquarks with different $SU(2)$ -quantum numbers. The latter is induced by interactions with the Higgs boson and arise after electroweak symmetry breaking, see the second reference in [41]. As a result, tensor operators in leptoquark models are suppressed by the vacuum expectation value of the Higgs $v = \langle H^0 \rangle = (2\sqrt{2}G_F)^{-1/2}$ over the scalar leptoquark mass m_S . Specifically for $b \rightarrow s\bar{l}$ transitions this yields the tensor coefficients

$$C_{T,T5}^l \propto \frac{(4\pi)^2}{e^2} \frac{\lambda_{l3}^* \lambda_{2l}}{V_{tb} V_{ts}^* G_F m_S^2 m_S^2}. \quad (6.12)$$

7. Summary

We thoroughly investigated the angular distributions in $\bar{B} \rightarrow K\bar{l}l$ decays in a model-independent way. We find that the $\cos\theta$ -dependence in the normalized $1/\Gamma_l d\Gamma_l/d\cos\theta$ spectrum, see (1.2), offers great opportunities to test the SM and search for NP. The requisite observables are the flat term in the distribution, $F_H^l/2$ and the forward-backward asymmetry A_{FB}^l . The coefficient of $\cos^2\theta$ is related to F_H^l . No powers of $\cos\theta$ greater than two appear in the $\bar{B} \rightarrow K\bar{l}l$ angular distribution up to higher dimensional operators not present in \mathcal{H}_{eff} (2.1)-(2.3) and QED corrections. Both are strongly suppressed by powers of the low energy masses and momenta over the scale of electroweak NP and by $\alpha_e/(4\pi)$, respectively.

In the SM, $F_H^l \propto m_l^2$, and F_H^e is negligible. The SM value for F_H^μ is small, order few percent, and can be cleanly predicted using QCDF for low dilepton masses with 2% accuracy, see Table 2. Taking into account subleading $1/E$ -corrections the uncertainty is conservatively inflated to $\sim 6\%$. The forward-backward asymmetry vanishes exactly in the SM up to the aforementioned higher order OPE and QED corrections. The α_e -corrections induce the parametrically leading contribution of the order $\alpha_e/(4\pi)$.

We also give SM predictions for the $B^- \rightarrow K^- \bar{\mu}\mu$ and $\bar{B}^0 \rightarrow K^0 \bar{\mu}\mu$ branching ratios. They have a substantial uncertainty of order 32% mostly from the form factor. On the other hand, the SM ratio of $\bar{B} \rightarrow K\bar{\mu}\mu$ to $\bar{B} \rightarrow K\bar{e}e$ decay rates, R_K^{SM} , equals one at the level of 10^{-4} . We show analytically at large recoil using form factor symmetry relations that the apparent huge suppression of lepton flavor effects in R_K^{SM} results from the cancellation of $\mathcal{O}(m_l^2)$ -corrections to leading order in $1/E$ and α_s in the $\bar{B} \rightarrow K\bar{l}l$ decay rate, see (5.1). In addition potentially large corrections to R_K can arise from collinear QED logarithms, whose actual net effect depends on experimental cuts [29]. The corresponding calculation for $\bar{B} \rightarrow K\bar{l}l$ decays has not been done.

Beyond the SM, the observables F_H^l , A_{FB}^l and R_K are sensitive to Higgs and tensor interactions. We work out NP signatures and correlations by taking into account existing data on $\mathcal{B}(\bar{B}_s \rightarrow \bar{l}l)$ and $\mathcal{B}(\bar{B} \rightarrow X_s \bar{l}l)$ for $l = e$ and $l = \mu$ separately. We find that the

NP modifications to the angular observables F_H^e , F_H^μ , A_{FB}^μ and $R_K - 1$ can be sizeable, see Table 5. Even larger effects in the forward-backward asymmetries A_{FB}^μ and A_{FB}^e arise in models where both (pseudo-) scalar and tensor operators are present. From a scan of twelve real NP coefficients $C_{S,P}^{l(l)}$, $C_{T,T5}^l$ for $l = e$ and $l = \mu$ we find model-independently the upper bounds

$$|A_{\text{FB}}^e| < 13\%, \quad |A_{\text{FB}}^\mu| < 15\%. \quad (7.1)$$

Both R_K and F_H^μ enable precision tests of the SM in exclusive $\bar{B} \rightarrow K\bar{l}l$ decays, but their experimental requirements are different: Whereas R_K requires only measurements of decay rates into both electrons and muons, F_H^μ is extracted from the muon channel alone, however, at the price of an angular analysis. The latter needs high statistics and is well suited for the LHC(b) setup. NP searches with angular distributions in $\bar{B} \rightarrow K\bar{\mu}\mu$ should also be feasible at the Tevatron, where CDF has recently measured $\mathcal{B}(B^+ \rightarrow K^+\bar{\mu}\mu)$ and $\mathcal{B}(B^0 \rightarrow K^{*0}\bar{\mu}\mu)$ [5].

The experimental situation for the observables F_H^l , A_{FB}^l and R_K is currently at a very early stage, see Table 3. In particular, all measurements average $l = e$ and $l = \mu$ final states except the ones of R_K [2, 4]. Ultimately all observations in rare semileptonic decays $\bar{B} \rightarrow K\bar{l}l$, $\bar{B} \rightarrow K^*\bar{l}l$ and $\bar{B} \rightarrow X_s\bar{l}l$ should be available for each lepton flavor separately since deviations from the SM could be l -dependent. For example, NP in the electron channel could escape the $\bar{B} \rightarrow K\bar{\mu}\mu$ decay studies completely implying also $R_K < 1$. Existing data on the $l = e$ modes are weaker than the corresponding ones for decays into muons, allowing for larger NP effects in the electron modes. In this way, $b \rightarrow s\bar{e}e$ induced channels such as $\bar{B} \rightarrow K\bar{e}e$ provide unique opportunities for the clean B factory environment. Appropriate cuts in q^2 should be taken into account to maximally exploit the theoretical predictions.

Acknowledgments

We are happy to thank Yuehong Xie for stimulating questions and Thorsten Feldmann and Uli Haisch for helpful communication. G.P. is supported by a grant from the G.I.F., the German-Israeli-Foundation for Scientific Research and Development. The work of C.B. is supported by the Bundesministerium für Bildung und Forschung, Berlin-Bonn. G.H. gratefully acknowledges the hospitality and stimulating atmosphere provided by the Aspen Center for Physics during the final phase of this work.

A. $\bar{B} \rightarrow K\bar{l}l$ Form factors

In this appendix we give definitions and properties of the heavy-to-light form factors for the $\bar{B} \rightarrow K$ transition at large recoil. The symmetry relations emerging in this region between the QCD form factors are reviewed including symmetry breaking corrections. Furthermore, details about the form factor f_+ from Light Cone Sum Rules calculations [26] can be found here.

The $\bar{B} \rightarrow K$ matrix elements are parametrized in terms of the three QCD form factors f_+ , f_0 and f_T as [42]

$$\langle K(p_K) | \bar{s} \gamma_\mu b | \bar{B}(p_B) \rangle = (2p_B - q)_\mu f_+(q^2) + \frac{M_B^2 - M_K^2}{q^2} q_\mu [f_0(q^2) - f_+(q^2)], \quad (\text{A.1})$$

$$\langle K(p_K) | \bar{s} i \sigma_{\mu\nu} q^\nu b | \bar{B}(p_B) \rangle = -[(2p_B - q)_\mu q^2 - (M_B^2 - M_K^2) q_\mu] \frac{f_T(q^2)}{M_B + M_K}. \quad (\text{A.2})$$

At leading order in the $1/E$ expansion $f_{+,0,T}(q^2)$ obey symmetry relations [11, 12] such that they all can be related to a single form factor denoted by $\xi_P(q^2)$. Within QCDF a factorization scheme has been chosen with $f_+(q^2) \equiv \xi_P(q^2)$ [12]. Including subleading corrections, the symmetry relations can be written as

$$\begin{aligned} \frac{f_0}{f_+} &= \frac{2E}{M_B} \left[1 + \mathcal{O}(\alpha_s) + \mathcal{O}\left(\frac{q^2}{M_B^2} \sqrt{\frac{\Lambda_{\text{QCD}}}{E}}\right) \right], \\ \frac{f_T}{f_+} &= \frac{M_B + M_K}{M_B} \left[1 + \mathcal{O}(\alpha_s) + \mathcal{O}\left(\sqrt{\frac{\Lambda_{\text{QCD}}}{E}}\right) \right], \end{aligned} \quad (\text{A.3})$$

up to higher order QCD, power and mixed corrections. The α_s -corrections from the soft-overlap and hard scattering contributions indicated in (A.3) have been calculated in QCDF and are given in [12]. These corrections are taken into account in the numerical analysis of this work. Analogous relations can be found in the framework of SCET using $\overline{\text{MS}}$ subtractions [15, 43]. The symmetry relation breaking corrections due to subleading orders in the Λ_{QCD}/E expansion have been considered for the soft-overlap part using SCET [44]. The corresponding corrections are indicated in (A.3). Note that the expansion parameter is rather $\sqrt{\Lambda_{\text{QCD}}/E}$ than Λ_{QCD}/E , and that for f_0/f_+ an additional suppression of q^2/M_B^2 appears. Subleading contributions from hard spectator scattering to (A.3) are unknown and arise at higher order, $\mathcal{O}(\alpha_s \sqrt{\Lambda_{\text{QCD}}/E})$.

The form factor symmetry relations (A.3) imply in the SM for $\bar{B} \rightarrow K \bar{l} l$ decays

$$\frac{q^2}{M_B^2} |\tilde{F}_P|^2 + 4|F_A|^2 + \frac{M_B^2 - M_K^2 + q^2}{M_B^2} 2\text{Re}(\tilde{F}_P F_A^*) = \mathcal{O}\left(\alpha_s, \frac{q^2}{M_B^2} \sqrt{\frac{\Lambda_{\text{QCD}}}{E}}\right), \quad (\text{A.4})$$

which enters $a_l^{\text{SM}} + c_l^{\text{SM}}$, see Section 4. Here, the explicit SM expressions for $F_{V,A,P}$ (3.2) have been used and $F_P = m_l \tilde{F}_P$ has been rescaled. The relation (A.4) involves only the ratio f_0/f_+ and results in a beneficial q^2/M_B^2 suppression of the power corrections. Beyond the SM the corresponding expression depends on all functions F_i and there are in general no cancellations from symmetry relations.

We employ the form factor $f_+(q^2) = \xi_P(q^2)$ from LCSR calculations [26]. It is given in terms of the Gegenbauer moments of the K -meson LCDA, a_1^K, a_2^K and a_4^K as

$$f_+(q^2) = f_+^{as}(q^2) + a_1^K(\mu_{IR}) f_+^{a_1}(q^2) + a_2^K(\mu_{IR}) f_+^{a_2}(q^2) + a_4^K(\mu_{IR}) f_+^{a_4}(q^2). \quad (\text{A.5})$$

The q^2 -dependent functions $f_+^{a_i}$, $i = 1, 2, 4$ and f_+^{as} are obtained from a fit and parametrized in [26]. Here we use ‘‘set 2’’ with $m_b^{\text{pole}} = 4.8$ GeV corresponding to the infrared factorization scale $\mu_{IR} = \sqrt{M_B^2 - m_b^{\text{pole}2}} = 2.2$ GeV. The running of the Gegenbauer moments given in Table 1 from 1 GeV to 2.2 GeV is accounted for by the scaling factors

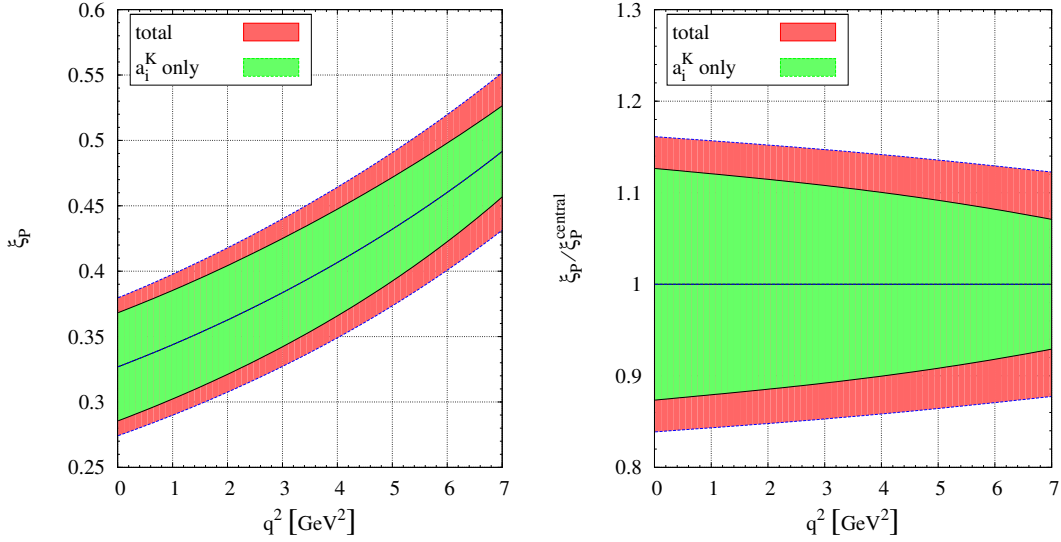


Figure 8: The form factor $\xi_P(q^2) = f_+(q^2)$ in the low- q^2 region including uncertainties from the Gegenbauer moments a_i^K (lighter shaded area) and from a_i^K and Δ_{as} with their uncertainties added in quadrature (darker shaded area), for details see text. In the left-hand plot is shown $\xi_P(q^2)$, and in the right-hand plot the form factor normalized to its central value, $\xi_P(q^2)/\xi_P^{\text{central}}(q^2)$.

$\{0.793, 0.696, 0.590\}$ for $\{a_1^K, a_2^K, a_4^K\}$. The relative uncertainty of f_+ due to the asymptotic form factor f_+^{as} (which is independent of the a_i^K) at $q^2 = 0$ is approximately $\Delta_{as}/f_+(0) = 10\%$, see Table 2 of [26]. In order to estimate the form factor uncertainty in the low- q^2 region we scan over the Gegenbauer moments according to the ranges in Table 1 translated to $\mu_{IR} = 2.2$ GeV and add the uncertainty from Δ_{as} in quadrature. The form factor $f_+(q^2) = \xi_P(q^2)$ with its uncertainties with and without Δ_{as} is shown in Figure 8. The total uncertainty is 16% at maximal recoil and reduces to 12% at $q^2 = 7$ GeV². The reduction of the relative form factor uncertainty towards larger values of q^2 stems from the increase of the form factor in this region while keeping Δ_{as} from $q^2 = 0$. The decrease of the form factor uncertainty for $q^2 > 0$ has been considered likely in [26].

B. \mathcal{T}_P for $\bar{B} \rightarrow K$

The amplitude $\mathcal{T}_P(q^2)$ can be extracted from [9] as

$$\begin{aligned} \mathcal{T}_P &= \xi_P \left[C_P^{(0)} + \frac{\alpha_s C_F}{4\pi} \left(C_P^{(f)} + C_P^{(\text{nf})} \right) \right] \\ &+ \frac{\pi^2 f_B f_K}{N_c M_B} \sum_{\pm} \int \frac{d\omega}{\omega} \Phi_{B,\pm}(\omega) \int_0^1 du \Phi_K(u) \left[T_{P,\pm}^{(0)} + \frac{\alpha_s C_F}{4\pi} \left(T_{P,\pm}^{(f)} + T_{P,\pm}^{(\text{nf})} \right) \right] (\omega, u), \end{aligned} \quad (\text{B.1})$$

where all $T_{P,\pm}^{(0)}$, $T_{P,\pm}^{(f)}$ and $T_{P,\pm}^{(\text{nf})}$ are functions of (ω, u) . f_B and f_K denote the B - and K -meson decay constants, respectively, whereas $\Phi_{B,\pm}(\omega)$ and $\Phi_K(u)$ are the corresponding

LCDA's. The remaining quantities are calculable perturbatively

$$C_P^{(0)} = -C_{\parallel}^{(0)}, \quad C_P^{(\text{nf})} = -C_{\parallel}^{(\text{nf})}, \quad T_{P,\pm}^{(0)} = -T_{\parallel,\pm}^{(0)}, \quad T_{P,\pm}^{(\text{nf})} = -T_{\parallel,\pm}^{(\text{nf})},$$

$$C_P^{(\text{f})} = -C_7^{\text{eff}} \left[4 \ln \frac{m_b^2}{\mu^2} + 2L - 4 + 4 \frac{\mu_f}{m_b} \right], \quad T_{P,+}^{(\text{f})} = -C_7^{\text{eff}} \frac{4M_B}{E(1-u)}, \quad T_{P,-}^{(\text{f})} = 0. \quad (\text{B.2})$$

Here the shift of the b -quark mass in \mathcal{O}_7 from the $\overline{\text{MS}}$ to the PS scheme has been taken into account in $C_P^{(\text{f})}$. All quantities $L, C_7^{\text{eff}}, C_{\parallel}^{(0)}, C_{\parallel}^{(\text{nf})}$ and $T_{\parallel,\pm}^{(0)}, T_{\parallel,\pm}^{(\text{nf})}$ in (B.2) are given in [9]. The expressions for $C_P^{(\text{f})}$ and $T_{P,+}^{(\text{f})}$ in (B.2) agree with $-C_{\parallel}^{(\text{f})}$ and $-T_{\parallel,+}^{(\text{f})}$ given in [10], respectively, where a different definition of the longitudinal form factor ξ_{\parallel} with respect to the one used in previous works [9, 12] is employed.

References

- [1] S. Hashimoto *et al.*, Letter of intent for KEK Super B Factory, KEK-REPORT-2004-4; J. L. Hewett *et al.*, The discovery potential of a Super B Factory, arXiv:hep-ph/0503261; M. Bona *et al.*, SuperB: A High-Luminosity Asymmetric e^+e^- Super Flavor Factory, arXiv:0709.0451 [hep-ex]; P. Koppenburg, CERN-LHCB-2007-034.
- [2] K. Abe *et al.* [Belle Collaboration], arXiv:hep-ex/0410006.
- [3] A. Ishikawa *et al.*, Phys. Rev. Lett. **96**, 251801 (2006) [arXiv:hep-ex/0603018].
- [4] B. Aubert *et al.* [BABAR Collaboration], Phys. Rev. D **73**, 092001 (2006) [arXiv:hep-ex/0604007].
- [5] F. Scuri [CDF Collaboration], arXiv:0705.3004 [hep-ex].
- [6] A. Ali, P. Ball, L. T. Handoko and G. Hiller, Phys. Rev. D **61**, 074024 (2000) [arXiv:hep-ph/9910221]; A. Ali, E. Lunghi, C. Greub and G. Hiller, Phys. Rev. D **66** (2002) 034002 [arXiv:hep-ph/0112300].
- [7] C. Bobeth, T. Ewerth, F. Kruger and J. Urban, Phys. Rev. D **64**, 074014 (2001) [arXiv:hep-ph/0104284].
- [8] G. Hiller and F. Kruger, Phys. Rev. D **69**, 074020 (2004) [arXiv:hep-ph/0310219].
- [9] M. Beneke, T. Feldmann and D. Seidel, Nucl. Phys. B **612**, 25 (2001) [arXiv:hep-ph/0106067].
- [10] M. Beneke, T. Feldmann and D. Seidel, Eur. Phys. J. C **41**, 173 (2005) [arXiv:hep-ph/0412400].
- [11] J. Charles, A. Le Yaouanc, L. Oliver, O. Pene and J. C. Raynal, Phys. Rev. D **60**, 014001 (1999) [arXiv:hep-ph/9812358].
- [12] M. Beneke and T. Feldmann, Nucl. Phys. B **592**, 3 (2001) [arXiv:hep-ph/0008255].
- [13] K. G. Chetyrkin, M. Misiak and M. Munz, Phys. Lett. B **400**, 206 (1997) [Erratum-ibid. B **425**, 414 (1998)] [arXiv:hep-ph/9612313].
- [14] F. Borzumati, C. Greub, T. Hurth and D. Wyler, Phys. Rev. D **62**, 075005 (2000) [arXiv:hep-ph/9911245].

- [15] C. W. Bauer, S. Fleming, D. Pirjol and I. W. Stewart, Phys. Rev. D **63**, 114020 (2001) [arXiv:hep-ph/0011336].
- [16] A. Ali, G. Kramer and G. h. Zhu, Eur. Phys. J. C **47**, 625 (2006) [arXiv:hep-ph/0601034]; K. S. M. Lee, Z. Ligeti, I. W. Stewart and F. J. Tackmann, Phys. Rev. D **75**, 034016 (2007) [arXiv:hep-ph/0612156].
- [17] A. J. Buras and M. Munz, Phys. Rev. D **52**, 186 (1995) [arXiv:hep-ph/9501281].
- [18] M. Beneke, Phys. Lett. B **434**, 115 (1998) [arXiv:hep-ph/9804241].
- [19] C. Bobeth, M. Misiak and J. Urban, Nucl. Phys. B **574**, 291 (2000) [arXiv:hep-ph/9910220]; P. Gambino, M. Gorbahn and U. Haisch, Nucl. Phys. B **673**, 238 (2003) [arXiv:hep-ph/0306079].
- [20] W. M. Yao *et al.* [Particle Data Group], J. Phys. G **33** (2006) 1 and 2007 partial update for edition 2008 (URL: <http://pdg.lbl.gov>).
- [21] CKMfitter webpage: <http://ckmfitter.in2p3.fr>; H. Lacker, arXiv:0708.2731 [hep-ph].
- [22] [CDF Collaboration], arXiv:hep-ex/0703034.
- [23] T. Onogi, PoS **LAT2006**, 017 (2006) [arXiv:hep-lat/0610115].
- [24] V. M. Braun, D. Y. Ivanov and G. P. Korchemsky, Phys. Rev. D **69**, 034014 (2004) [arXiv:hep-ph/0309330].
- [25] P. Ball, V. M. Braun and A. Lenz, JHEP **0605**, 004 (2006) [arXiv:hep-ph/0603063].
- [26] P. Ball and R. Zwicky, Phys. Rev. D **71**, 014015 (2005) [arXiv:hep-ph/0406232].
- [27] H. H. Asatrian, H. M. Asatrian, C. Greub and M. Walker, Phys. Lett. B **507**, 162 (2001) [arXiv:hep-ph/0103087]; H. H. Asatryan, H. M. Asatrian, C. Greub and M. Walker, Phys. Rev. D **65**, 074004 (2002) [arXiv:hep-ph/0109140]; A. Ghinculov, T. Hurth, G. Isidori and Y. P. Yao, Nucl. Phys. B **685**, 351 (2004) [arXiv:hep-ph/0312128].
- [28] C. Bobeth, P. Gambino, M. Gorbahn and U. Haisch, JHEP **0404**, 071 (2004) [arXiv:hep-ph/0312090].
- [29] T. Huber, E. Lunghi, M. Misiak and D. Wyler, Nucl. Phys. B **740**, 105 (2006) [arXiv:hep-ph/0512066].
- [30] P. Krawczyk, Z. Phys. C **44**, 509 (1989); W. Skiba and J. Kalinowski, Nucl. Phys. B **404**, 3 (1993).
- [31] J. F. Donoghue and F. Gabbiani, Phys. Rev. D **51**, 2187 (1995) [arXiv:hep-ph/9408390].
- [32] "Rare B_s and D decays with the $D\bar{O}$ detector" Talk given by A. Maciel at HEP 2007, July 20, 2007, Parallel Session "Flavour physics and CP violation".
- [33] M. Acciarri *et al.* [L3 Collaboration], Phys. Lett. B **391**, 474 (1997).
- [34] B. Aubert *et al.* [BABAR Collaboration], Phys. Rev. Lett. **93**, 081802 (2004) [arXiv:hep-ex/0404006]; K. Abe *et al.* [Belle Collaboration], arXiv:hep-ex/0408119; M. Iwasaki *et al.* [Belle Collaboration], Phys. Rev. D **72**, 092005 (2005) [arXiv:hep-ex/0503044].
- [35] S. Fukae, C. S. Kim, T. Morozumi and T. Yoshikawa, Phys. Rev. D **59**, 074013 (1999) [arXiv:hep-ph/9807254].

- [36] P. H. Chankowski and L. Slawianowska, *Eur. Phys. J. C* **33**, 123 (2004) [arXiv:hep-ph/0308032].
- [37] D. A. Demir, K. A. Olive and M. B. Voloshin, *Phys. Rev. D* **66**, 034015 (2002) [arXiv:hep-ph/0204119].
- [38] Christoph Bobeth and Thorsten Ewerth, private notes.
- [39] Y. Grossman, Z. Ligeti and E. Nardi, *Phys. Rev. D* **55** (1997) 2768 [arXiv:hep-ph/9607473].
- [40] Y. G. Xu, R. M. Wang and Y. D. Yang, *Phys. Rev. D* **74**, 114019 (2006) [arXiv:hep-ph/0610338].
- [41] S. Davidson, D. C. Bailey and B. A. Campbell, *Z. Phys. C* **61**, 613 (1994) [arXiv:hep-ph/9309310]; M. Hirsch, H. V. Klapdor-Kleingrothaus and S. G. Kovalenko, *Phys. Lett. B* **378**, 17 (1996) [arXiv:hep-ph/9602305].
- [42] M. Wirbel, B. Stech and M. Bauer, *Z. Phys. C* **29**, 637 (1985); N. Isgur and M. B. Wise, *Phys. Rev. D* **42**, 2388 (1990).
- [43] R. J. Hill, T. Becher, S. J. Lee and M. Neubert, *JHEP* **0407**, 081 (2004) [arXiv:hep-ph/0404217].
- [44] M. Beneke, A. P. Chapovsky, M. Diehl and T. Feldmann, *Nucl. Phys. B* **643**, 431 (2002) [arXiv:hep-ph/0206152].